

1 *Type of the Paper: Article*

## 2 **Comb-like dextran copolymers: A versatile strategy to** 3 **coat highly porous MOF nanoparticles with a PEG** 4 **shell**

5 **Giovanna Cutrone<sup>1†</sup>, Jingwen Qiu<sup>2†</sup>, Mario Menendez-Miranda<sup>2</sup>, Juan M. Casas-Solvas<sup>1</sup>, Ahmet**  
6 **Aykaç<sup>1</sup>, Xue Li<sup>2</sup>, Daniel Foulkes<sup>2</sup>, Borja Moreira-Alvarez<sup>3</sup>, Jorge Ruiz Encinar<sup>3</sup>, Catherine**  
7 **Ladavière<sup>4</sup>, Didier Desmaële<sup>5</sup>, Antonio Vargas-Berenguel<sup>1,\*</sup> and Ruxandra Gref<sup>2,\*</sup>**

8 <sup>1</sup> Department of Chemistry and Physics, University of Almería, Ctra. de Sacramento s/n, 04120 Almería,  
9 Spain; cutrone@ual.es (G.C.); [jmccasas@ual.es](mailto:jmccasas@ual.es) (J.M.C.-S.); [ahmet.aykac@ikc.edu.tr](mailto:ahmet.aykac@ikc.edu.tr) (A.A.)

10 <sup>2</sup> Institute of Molecular Sciences, UMR CNRS 8214, Université Paris-Sud, Université Paris Saclay, 91400 Orsay,  
11 France; jingwen.qiu@u-psud.fr (J.Q.); mario.menendez-miranda@u-psud.fr (M.M.-M.); xue.li@u-psud.fr  
12 (X.L.); Daniel.Foulkes@liverpool.ac.uk (D.F.)

13 <sup>3</sup> Department of Physical and Analytical Chemistry, University of Oviedo, Julián Clavería 8, 33006 Oviedo,  
14 Spain; borjamoreira@gmail.com (B.M.-A.); ruizjorge@uniovi.es (J.R.E.)

15 <sup>4</sup> University of Lyon, CNRS, UMR 5223, IMP, 15 bd André Latarjet, F-69622 Villeurbanne, France;  
16 catherine.ladaviere@univ-lyon1.fr

17 <sup>5</sup> Institut Galien Paris-Sud, UMR 8612, CNRS, Université Paris-Sud, Faculté de Pharmacie, 5 rue JB Clément,  
18 92296 Châtenay-Malabry, France; didier.desmaele@u-psud.fr

19

20 \* Correspondence: ruxandra.gref@u-psud.fr (R.G.); Tel.: +33 1 69 15 82 34 (R.G.)

21 (A. V.-B.); Tel.: +34 950015315 (A. V.-B.);

22

23 † These authors equally contributed to this work.

24 Received: date; Accepted: date; Published: date

### 25 **Abstract:**

26 Nanoparticles made of metal-organic frameworks (nanoMOFs) are becoming of increasing interest  
27 as drug carriers. However, preventing nanoMOFs recognition and clearance by the innate immune  
28 system, a prerequisite for biomedical applications, presents an important challenge. In this study  
29 we provide a proof of concept that the outer surface of biocompatible iron-based nanoMOFs can be  
30 functionalized in a rapid, organic solvent-free and non-covalent manner using a novel family of  
31 comb-like copolymers made of dextran (DEX) grafted with both poly(ethylene glycol) (PEG) and  
32 alendronate (ALN) moieties. We describe the synthesis and full characterization of DEX-PEG-ALN  
33 copolymers by click chemistry, with control of both the amount of grafted PEG and ALN moieties.  
34 The copolymers, freely soluble in aqueous media, were used to directly coat the nanoMOFs in water  
35 by simple incubation at room temperature. The coating procedure did not affect the nanoMOFs'  
36 morphology nor their crystalline structure. As strong iron complexing groups, the ALN moieties  
37 ensured multiple cooperative anchoring of the copolymers to the nanoMOFs surface, resulting in  
38 stable coatings that substantially decreased their internalization by macrophages *in vitro*, providing  
39 new perspectives for biomedical applications.

40 **Keywords:** metal organic frameworks; nanoparticles; surface modification; dextran; poly(ethylene  
41 glycol); macrophage uptake; click chemistry.

42

## 43 1. Introduction

44 Metal-organic frameworks (MOFs) are one of the latest classes of ordered porous solids which  
45 have attracted growing interest since their discovery in 1989 [1], in reason of their remarkable  
46 versatility. Indeed, almost any metal could be associated to polycomplexing linkers such as  
47 carboxylates, phosphonates, sulfonates or imidazolates leading to the discovery of thousands of  
48 MOFs with a variety of pore sizes and shapes [2,3]. Among the MOF family, nanosized MOFs  
49 (nanoMOFs) based on porous iron(III) polycarboxylates have emerged as an important class of  
50 biodegradable and non-toxic [4,5] materials that can be loaded with exceptional quantities (within  
51 the 20–70 wt% range) of a large variety of therapeutic agents [4,6]. This paved the way to novel  
52 perspectives in terms of targeted delivery of drugs [7,8] and theranostics [4]. For biomedical  
53 applications, it is of utmost importance to engineer the surface of the nanoMOFs, since the *in vivo* fate  
54 of any nanoparticle in the living body (biodistribution, pharmacokinetics and targeting abilities)  
55 depends upon its surface physicochemical properties. For instance, it was shown that surface  
56 functionalization with hydrophilic polymers such as poly(ethylene glycol) (PEG) in a “brush”  
57 configuration could dramatically extend the blood circulation times of nanoparticles by mitigating  
58 their recognition by the reticuloendothelial system [9,10]. However, to date, Doxil® represents the  
59 only FDA-approved PEGylated liposome-based nanocarrier of anticancer drug (Doxorubicin) [11].

60 Functionalization of nanoMOF surfaces will be critical to their success as potential nanocarriers  
61 in therapeutic contexts. However, thus far, only a limited number of cases have been reported that  
62 have aimed to modify the surface of nanoMOFs with PEG shells [12–16]. As compared to dense  
63 nanoparticles made of biodegradable polymers or liposomes, the porous surface of MOFs is a  
64 challenging surface to functionalize. Indeed, it was reported that PEG chains are able to penetrate  
65 within the pores, blocking them and/or decreasing the drug loading capacity [12]. To avoid PEG  
66 penetration into the highly porous MOFs, PEG-based shells were formed by GraftFast, a method  
67 involving polymerization of acryl PEGs [14]. By this way, PEG derivatives with initial molecular  
68 weights of 480, 2000 and 5000 Da were polymerized leading to stable coatings. However, the  
69 molecular weight of the resulting PEG-based copolymer could not be efficiently controlled. Another  
70 recent strategy employed cyclodextrin (CD) derivatives, which were first adsorbed onto the MOFs’  
71 surfaces prior to complex formation with PEG grafted with adamantane moieties [14]. However, the  
72 two-step procedure required by this method resulted in a difficulty to control the quantity of grafted  
73 PEG.

74 Moreover, no study has yet demonstrated that a PEG coating on nanoMOFs could effectively  
75 reduce their reticuloendothelial sequestration. In this context, there is still a clear demand to engineer  
76 versatile PEG-based coatings onto the nanoMOF surface, with proof of concept, by reducing uptake  
77 by macrophages. Here we address this challenge by using a novel family of copolymers, synthesized  
78 by grafting onto a dextran (DEX) backbone two types of moieties: i) PEG chains to avoid macrophage  
79 uptake and ii) alendronate (ALN) to spontaneously coordinate to the nanoMOFs surface. Iron  
80 trimesate MIL-100(Fe) (MIL stands for Material of the Institute Lavoisier) nanoMOFs were selected  
81 as core materials, in reason of their biodegradability, capacity to incorporate a series of drugs  
82 (antibiotics [17], anticancer drugs [18,19], anti-infective agents [6,20]) reaching unprecedented  
83 payloads together with controlled releases, versatility in terms of drug loadings and lack of *in vivo*  
84 toxicity [5,21].

85 Here we show the possibility to achieve stable coatings by a straightforward method, based on  
86 cooperative interactions between the ALN moieties and the external surface of MIL-100(Fe)  
87 nanoMOFs. Thus, we describe the synthetic strategies to control both PEG and ALN densities on the

88 DEX backbone, as well as the convenient one-step method to coat the nanoMOFs. The PEG “brush”  
89 efficiently reduced macrophage uptake as demonstrated by both microscopic investigations and  
90 quantitative ICP-MS determination of the amount of internalized nanoMOFs.

91

## 92 2. Materials and Methods

### 93 2.1 Chemicals and general methods

94 Thin layer chromatography (TLC) was performed on Merck silica gel 60 F<sub>254</sub> aluminum sheets  
95 and developed by UV–vis light, iodine, 5% v/v sulfuric acid in ethanol, 5% w/v phosphomolybdic  
96 acid in ethanol, and 1% w/v potassium permanganate in aqueous 0.1% w/v NaOH containing 7% w/v  
97 potassium carbonate, depending on the case. Flash column chromatography was performed on  
98 Merck silica gel (230–400 mesh, ASTM). Infrared spectra were recorded on a Bruker Alpha FTIR  
99 equipped with a Bruker universal ATR sampling accessory. <sup>1</sup>H, <sup>13</sup>C, <sup>31</sup>P and 2D NMR spectra were  
100 recorded on a Bruker Avance III HD 600 MHz spectrometer equipped with a QCI <sup>1</sup>H/<sup>13</sup>C/<sup>15</sup>N/<sup>31</sup>P  
101 proton-optimized quadrupole inverse cryoprobe with <sup>1</sup>H and <sup>13</sup>C cryochannels, or a Bruker Nanobay  
102 Avance III HD 300 MHz spectrometer equipped with a QNP <sup>1</sup>H/<sup>13</sup>C/<sup>19</sup>F/<sup>31</sup>P probe, depending on the  
103 sample. Standard Bruker software was used for acquisition and processing routines. Chemical shifts  
104 ( $\delta$ ) are given in parts per million (ppm) and referenced to internal tetramethylsilane (TMS) signal ( $\delta_{\text{H}}$ ,  
105  $\delta_{\text{C}}$  0.00). *J* values are given in hertz (Hz). ESI-TOF mass spectra were recorded on a Agilent LC/MSD-  
106 TOF spectrometer in both positive and negative modes. Syringe filtering was conducted using nylon  
107 0.45  $\mu\text{m}$  Milipore Millex<sup>®</sup> syringe-driven filter units. Dialysis was performed using Medicell  
108 Membranes Ltd 12000-14000 Da molecular weight cutoff (MWCO) Visking dialysis tubing. Elemental  
109 analyses were recorded on an Elementar Vario Micro CHNS analyzer. HR-ICP-MS results were  
110 obtained by using a Thermo Finnigan magnetic sector field ELEMENT 2 inductively coupled plasma  
111 mass spectrometer. A Hanna HI 98192 EC/TDS/NaCl/Resistivity meter was employed to monitor  
112 dialysate solutions conductivity during dialysis.

113 6-Bromohexanoic acid (Aldrich, 97%), sodium azide (Panreac, 99%), *N*-hydroxysuccinimide  
114 (NHS, Aldrich, 98%), *N*-(3-dimethylaminopropyl)-*N'*-ethylcarbodiimide hydrochloride (EDC, Fluka,  
115  $\geq 98\%$ ), alendronic acid monosodium salt trihydrate (CarboSynth, purum), poly(ethylene glycol)  
116 methyl ether (MeOPEG<sub>45</sub>OH, Aldrich, Mn  $\sim 2000$ ), 4-dimethylaminopyridine (DMAP, Fluka,  $\geq 98\%$ ),  
117 methanesulfonyl chloride (MsCl, Fluka,  $\geq 99\%$ ), 1,1'-carbonyldiimidazole (CDI, Acros, 97%),  
118 propargylamine (Aldrich, 98%), anhydrous copper(II) sulfate (Fluka, 98%), (+)-sodium L-ascorbate  
119 (Sigma, BioXtra,  $\geq 99\%$ ), and ethylenediaminetetraacetic acid disodium salt dihydrate (EDTA, Fluka,  
120 purum) were purchased from commercial sources and used without further purification otherwise  
121 indicated. Anhydrous LiCl (Sigma-Aldrich, 99%) and dextran T-40 (Pharmacosmos, purum,  
122 Nominative Mw 40000 Da) were purchased from commercial sources and dried at 80 °C under high  
123 vacuum for 48 h in the presence of P<sub>2</sub>O<sub>5</sub> prior to use. Triethylamine (Sigma-Aldrich,  $>99\%$ ) and  
124 organic solvents were dried according to literature procedures [22]. Dry DMF (AcroSeal, 99.8%, over  
125 molecular sieves) was purchased from Acros. Iron (III) chloride hexahydrate (Alfa Aesar,  
126 Schiltigheim, France, 98%), 1,3,5-benzenetricarboxylic acid (BTC, Sigma-Aldrich, Saint-Quentin-  
127 Fallavier, France, 95%) and absolute ethanol (Carlo Erba, Val-de-Reuil, France, 99%,) were used for  
128 the synthesis of nanoMOFs. Potassium chloride (Sigma-Aldrich, XX%) was used for nanoMOFs Zeta  
129 potential (ZP) measurements. Human serum albumin (HSA, Sigma-Aldrich) and biconchonic acid  
130 (BCA) protein assay kit (Pierce™ Thermo Fisher) was used for HSA adsorption test. Deionized Milli-  
131 Q water was obtained from a Millipore apparatus with a 0.22  $\mu\text{m}$  filter.

132 **Number average molecular weight analysis.** The number average molecular weight (*M<sub>n</sub>*) and  
133 the molar-mass dispersity values of dextran derivatives **5** and **7** were measured by using a SEC  
134 column (TSKgel G2500PW and G6000PW columns) coupled with a differential refractometer (RI,  
135 Optilab T-rEX, Wyatt Technology) with a laser at  $\lambda = 658 \text{ nm}$ , thermostated at 25°C, and a multi-angle

136 laser light scattering instrument (MALLS, HELEOS II, Wyatt Technology) equipped with a laser  
137 operating at  $\lambda = 664$  nm. Degassed and filtered (0.1  $\mu\text{m}$  membrane) 0.15 M ammonium acetate/0.20  
138 M acetic acid buffer (pH = 4.5) was used as eluent at a flow rate of 0.5 mL/min (with a refractive index  
139 increment value,  $dn/dc$  of 0.147 ml/g for dextran). These eluents were also used as solvent of samples,  
140 and the resulting solutions were filtered on a 0.45  $\mu\text{m}$  membrane before injection. Finally, 200  $\mu\text{L}$  of  
141 each sample at 1 mg/mL were injected. The data have been exploited thanks to the ASTRA 6.1.7.17  
142 software (Wyatt Technology).

143 **Cell culture.** Murine macrophage cell line J774A.1 (ATCC) were grown in Dulbecco's Modified  
144 Eagle's Medium (Thermo Fischer) supplemented with 10% v/v decomplexed fetal bovine serum  
145 (FBS) at 37 °C in humidified conditions with 5% CO<sub>2</sub>. Prussian blue iron staining kit (Sigma-Aldrich)  
146 containing potassium ferrocyanide, pararosaniline and hydrochloric acid was used for cell staining..

147

## 148 2.2 Synthesis and characterization of dextran-PEG

149 **2.2.1 Synthesis of 6-azidohexanoic acid (1):** Compound 1 was prepared as described in literature  
150 [23,24] with small modifications. Specifically, NaN<sub>3</sub> (1 g, 15.4 mmol) was added to a solution of 6-  
151 bromohexanoic acid (1.5 g, 7.7 mmol) in dry DMF (10 mL) under N<sub>2</sub> atmosphere and stirred at 85 °C  
152 overnight until TLC (2:1 hexane:EtOAc) showed complete disappearance of the starting material and  
153 the appearance of a spot at  $R_f = 0.59$ . The solvent was rotary evaporated under high vacuum and the  
154 residue was dissolved in H<sub>2</sub>O (20 mL) and extracted with EtOAc (3x30 mL). The organic layers were  
155 combined, dried (MgSO<sub>4</sub>), and rotary evaporated to give 6-azidohexanoic acid 1 (0.866 g, 5.5 mmol,  
156 70%) as slightly yellow oil. NMR data agreed with those previously reported [24]: <sup>1</sup>H NMR (300 MHz,  
157 CDCl<sub>3</sub>)  $\delta$  (ppm): 11.04 (s, 1H, COOH), 3.24 (t, 2H, <sup>3</sup>J = 6.9 Hz, CH<sub>2</sub>N<sub>3</sub>), 2.32 (t, 2H, <sup>3</sup>J = 7.3 Hz,  
158 CH<sub>2</sub>COOH), 1.70-1.50 (m, 4H, CH<sub>2</sub>CH<sub>2</sub>COOH, CH<sub>2</sub>CH<sub>2</sub>N<sub>3</sub>), 1.40 (m, 2H, CH<sub>2</sub>CH<sub>2</sub>CH<sub>2</sub>N<sub>3</sub>); <sup>13</sup>C NMR (75  
159 MHz, CDCl<sub>3</sub>)  $\delta$  (ppm): 179.1 (COOH), 51.2 (CH<sub>2</sub>N<sub>3</sub>), 34.0 (CH<sub>2</sub>COOH), 28.6 (CH<sub>2</sub>CH<sub>2</sub>N<sub>3</sub>), 26.2  
160 (CH<sub>2</sub>CH<sub>2</sub>CH<sub>2</sub>N<sub>3</sub>), 24.3 (CH<sub>2</sub>CH<sub>2</sub>COOH).

161 **2.2.2. Synthesis of 2,5-dioxopyrrolidin-1-yl 6-azidohexanoate (2):** Compound 2 was prepared  
162 as described in literature [25] with small modifications. Specifically, *N*-hydroxysuccinimide (520 mg,  
163 4.5 mmol) was added to a solution of 6-azidohexanoic acid 1 (650 mg, 4.1 mmol) in dry CH<sub>2</sub>Cl<sub>2</sub> (10  
164 mL) under N<sub>2</sub> atmosphere at room temperature and the mixture was stirred until complete  
165 solubilisation. Then, EDC (860 mg, 4.5 mmol) was added and the solution was stirred at room  
166 temperature until TLC (2:1 hexane:EtOAc) showed complete disappearance of the starting material  
167 and the appearance of a spot at  $R_f = 0.41$ . After 16h, the mixture was washed with 1 N HCl (2x15 mL)  
168 and saturated aq. NaHCO<sub>3</sub> (2x15 mL). The aqueous layer was extracted with CH<sub>2</sub>Cl<sub>2</sub> (2x10 mL). All  
169 organic phases were combined, dried (MgSO<sub>4</sub>), and rotary evaporated. The residue was purified by  
170 column chromatography using 2:1 hexane:EtOAc as eluent to yield compound 2 (790 mg, 3.1 mmol,  
171 76%) as a colourless liquid. NMR data agreed with those previously reported [25]: <sup>1</sup>H NMR (300 MHz,  
172 CDCl<sub>3</sub>)  $\delta$  (ppm): 3.23 (t, 2H, <sup>3</sup>J = 6.7 Hz, CH<sub>2</sub>N<sub>3</sub>), 2.75 (s, 4H, COCH<sub>2</sub>CH<sub>2</sub>CO), 2.56 (t, 2H, <sup>3</sup>J = 7.3 Hz,  
173 CH<sub>2</sub>COO), 1.90-1.30 (m, 6H, CH<sub>2</sub>CH<sub>2</sub>CH<sub>2</sub>CH<sub>2</sub>N<sub>3</sub>); <sup>13</sup>C NMR (75 MHz, CDCl<sub>3</sub>)  $\delta$  (ppm): 169.1  
174 (NCOCH<sub>2</sub>), 168.4 (COO), 51.1 (CH<sub>2</sub>N<sub>3</sub>), 30.8 (CH<sub>2</sub>COO), 28.4 (CH<sub>2</sub>), 25.9 (CH<sub>2</sub>), 25.6 (COCH<sub>2</sub>CH<sub>2</sub>CO),  
175 24.1 (CH<sub>2</sub>).

176 **2.2.3. Synthesis of the sodium salt of [4-(6-azidohexanamido)-1-hydroxy-1-(hydroxy-oxido-  
177 phosphoryl)-butyl]phosphonic acid (3):** Aqueous 0.1 M NaOH (~32 mL) was added dropwise to a  
178 suspension of alendronic acid monosodium salt trihydrate (0.83 g, 2.56 mmol) in MilliQ water (18  
179 mL) until pH ~8.5, forming a clear solution. A solution of 2,5-dioxopyrrolidin-1-yl 6-azidohexanoate  
180 2 (0.78 g, 3.1 mmol) in acetonitrile (18 mL) was added in four portions each 15 min. Before each  
181 portion, pH was measured and readjusted to ~8.5 with aqueous 0.1 M NaOH if needed. The reaction  
182 mixture was stirred overnight at room temperature and then the solvent was rotary evaporated. The  
183 residue was purified by a short column chromatography using 5:1 → 2:1 CH<sub>3</sub>CN:H<sub>2</sub>O as eluent to yield

184 compound **3** (0.84 g, 2.05 mmol, 80%) as a white solid after lyophilising: FT-IR (KBr)  $\nu/\text{cm}^{-1}$ : 3445,  
185 2938, 2867, 2100, 1632, 1558, 1105, 913, 620, 551;  $^1\text{H}$  NMR (600 MHz,  $\text{D}_2\text{O}$ )  $\delta$  (ppm): 3.34 (t, 2H,  $^3J =$   
186 6.9 Hz,  $\text{CH}_2\text{N}_3$ ), 3.22 (t, 2H,  $^3J = 6.8$  Hz,  $\text{CONHCH}_2$ ), 2.28 (t, 2H,  $^3J = 7.5$  Hz,  $\text{CH}_2\text{CONH}$ ), 2.01-1.93 (m,  
187 2H,  $\text{CH}_2\text{C}$ ), 1.86-1.81 (m, 2H,  $\text{CH}_2\text{CH}_2\text{C}$ ), 1.66-1.61 (m, 4H,  $\text{CH}_2\text{CH}_2\text{CONH}$ ,  $\text{CH}_2\text{CH}_2\text{N}_3$ ), 1.42-1.37 (m,  
188 2H,  $\text{CH}_2\text{CH}_2\text{CH}_2\text{N}_3$ );  $^{13}\text{C}$  NMR (150 MHz,  $\text{D}_2\text{O}$ )  $\delta$  (ppm): 176.9 (CONH), 73.9 (t,  $^1J_{\text{CP}} = 134.2$  Hz,  
189  $\text{C}(\text{PO}_3)_2$ ), 51.0 ( $\text{CH}_2\text{N}_3$ ), 40.0 ( $\text{NHCH}_2$ ), 36.6 ( $\text{CH}_2\text{CONH}$ ), 31.1 ( $\text{CH}_2\text{C}$ ), 27.7 ( $\text{CH}_2\text{CH}_2\text{N}_3$ ), 25.4  
190 ( $\text{CH}_2\text{CH}_2\text{CH}_2\text{N}_3$ ), 24.9 ( $\text{CH}_2\text{CH}_2\text{CONH}$ ), 23.4 (t,  $^3J_{\text{CP}} = 5.9$  Hz,  $\text{CH}_2\text{CH}_2\text{C}$ );  $^{31}\text{P}$  (242.9 MHz,  $\text{D}_2\text{O}$ )  $\delta$  (ppm):  
191 18.2 ( $\text{C}(\text{PO}_3)_2$ ); [ESI-TOF-MS] $^-$   $m/z$  calcd for  $\text{C}_{10}\text{H}_{21}\text{N}_4\text{O}_8\text{P}_2$  387.0840, found 387.0839 [M - Na];  $m/z$  calcd  
192 for  $\text{C}_{10}\text{H}_{20}\text{N}_4\text{O}_8\text{P}_2\text{Na}$  409.0660, found 409.0657 [M - H]; [ESI-TOF-MS] $^+$   $m/z$  calcd for  $\text{C}_{10}\text{H}_{22}\text{N}_4\text{O}_8\text{P}_2\text{Na}$   
193 411.0816 found 411.0818 [M + H] $^+$ ;  $m/z$  calcd for  $\text{C}_{10}\text{H}_{21}\text{N}_4\text{O}_8\text{P}_2\text{Na}_2$  433.0635, found 433.0643 [M + Na] $^+$ ;  
194  $m/z$  calcd for  $\text{C}_{10}\text{H}_{20}\text{N}_4\text{O}_8\text{P}_2\text{Na}_3$  455.0455 found 455.0465 [M - H + 2Na] $^+$ ;  $m/z$  calcd for  $\text{C}_{10}\text{H}_{19}\text{N}_4\text{O}_8\text{P}_2\text{Na}_4$   
195 477.0274, found 477.0283 [M - 2H + 3Na] $^+$ .

196 **2.2.4. Synthesis of 1-azido-1-deoxy- $\omega$ -O-methoxy-pentatetracontaethylene glycol (4):** A  
197 solution of MeOPEG<sub>45</sub>OH (35 g, 17.375 mmol), DMAP (428 mg, 3.5 mmol) and distilled Et<sub>3</sub>N (5.6 mL,  
198 40.250 mmol) in  $\text{CH}_2\text{Cl}_2$  (40 mL) was cooled to 0 °C under inert atmosphere. MsCl (2.7 mL, 35 mmol)  
199 was added dropwise over 15 min and the mixture was stirred at 0 °C during 30 min and then kept  
200 overnight at room temperature. The reaction mixture was then diluted with  $\text{CH}_2\text{Cl}_2$  (50 mL), and  
201 washed with 5 % v/v aqueous HCl solution (3x50 mL) and brine (50 mL). The organic phase was  
202 dried over  $\text{MgSO}_4$ , filtered and concentrated under reduced pressure to dryness. The solid was  
203 subsequently dissolved in dry DMF (40 mL) and  $\text{NaN}_3$  (2.276 g, 35 mmol) was added. The mixture  
204 was stirred at 60 °C for 24 h before the solvent was rotary evaporated under high vacuum. The residue  
205 was suspended in THF (20 mL) and sonicated (5 min), and filtered off. The clear organic filtrate was  
206 rotary evaporated, and the resulting solid was suspended in Et<sub>2</sub>O (50 mL), sonicated (5 min) and  
207 filtered. The solid was dissolved in H<sub>2</sub>O (100 mL) and extracted with  $\text{CH}_2\text{Cl}_2$  (3x100 mL). The organic  
208 phases were combined, dried ( $\text{MgSO}_4$ ) and rotary evaporated, and the residue dried under vacuum  
209 to give compound **4** (26.225 g, 12.858 mmol, 74 %) as a slightly yellow powder: FT-IR (KBr)  $\nu/\text{cm}^{-1}$ :  
210 2868, 2105, 1093, 948, 842, 729;  $^1\text{H}$  NMR (300 MHz,  $\text{D}_2\text{O}$ )  $\delta$ : 3.96-3.93 (m,  $^1J_{\text{H,C}} = 143.4$  Hz,  $^{13}\text{C}$  satellite  
211 peak), 3.75-3.68 (m, 176H,  $\text{OCH}_2\text{CH}_2\text{O}$ ), 3.65-3.61 (m, 2H,  $\text{CH}_2\text{CH}_2\text{N}_3$ ), 3.53-3.49 (m, 2H,  $\text{CH}_2\text{N}_3$ ), 3.49-  
212 3.46 (m,  $^1J_{\text{H,C}} = 71.7$  Hz,  $^{13}\text{C}$  satellite peak), 3.38 (s,  $\text{CH}_3\text{O}$ );  $^{13}\text{C}$  NMR (75 MHz,  $\text{D}_2\text{O}$ )  $\delta$ : 71.7 ( $\text{MeOCH}_2$ ),  
213 70.3 ( $\text{OCH}_2\text{CH}_2\text{O}$ ), 70.2 ( $\text{MeOCH}_2\text{CH}_2\text{O}$ ), 70.0 ( $\text{OCH}_2\text{CH}_2\text{N}_3$ ), 58.8 (OMe), 50.9 ( $\text{CH}_2\text{N}_3$ ).

214 **2.2.5. Synthesis of dextran propargylcarbamate (DEX-PC, 5):** LiCl (1 g) and dextran T-40 (4 g)  
215 were pre-dried at 80 °C in a high vacuum oven for 2 days in the presence of  $\text{P}_2\text{O}_5$ . The mixture was  
216 further dried by suspension in dry toluene (50 mL) and subsequent vacuum distillation at 50 °C. This  
217 azeotropic drying process with toluene was repeated twice, and then with anhydrous DMF (1x50  
218 mL) followed by evaporation of the solvent through a rotary evaporator at 60 °C under high vacuum.  
219 The dry mixture was finally dissolved in anhydrous DMF (80 mL) and stirred at 80 °C for 1.5 h. The  
220 solution was cooled down to room temperature before carbonyldiimidazole (0.972 g, 0.006 mmol)  
221 was added, and stirred for 2.5 h. Propargylamine (3.85 mL, 0.06 mmol) was then added and the  
222 mixture stirred at room temperature for 24 h. The solvent volume was reduced to 60 mL by rotary  
223 evaporation and the solution was poured into isopropanol (0.9 L). The resulting pale yellow solid  
224 was collected by filtration and dissolved in H<sub>2</sub>O (100 mL), syringe filtered (0.45  $\mu\text{m}$ ) and dialyzed  
225 (12000-14000 Da MWCO) against distilled water, changing dialysate solution each 3 hours until its  
226 conductivity was stable and below 1  $\mu\text{S}/\text{cm}$  (3 days for final value of 0.90  $\mu\text{S}/\text{cm}$ ) to yield DEX-PC **5**  
227 (3.6 g) as a white solid after lyophilization: FT-IR (KBr)  $\nu/\text{cm}^{-1}$ : 3420, 2930, 1709, 1639, 1530, 1461, 1419,  
228 1346, 1264, 1156, 1041, 1014, 766, 549, 527;  $^1\text{H}$  NMR (600 MHz,  $\text{D}_2\text{O}$ )  $\delta$  (ppm): 5.36 (d,  $^3J_{1,2} = 3.8$  Hz,  
229  $\alpha(1\rightarrow3,4)$  H-1), 5.21 (app bd,  $J_{\text{app}} = 2.8$  Hz,  $\alpha$  reducing end H-1,  $\text{CH-OCONH}$ ), 5.06 (d,  $^3J_{1,2} = 2.6$  Hz, H-  
230 1 $^{\text{s}}$ ), 5.01 (d,  $^3J_{1,2} = 3.0$  Hz,  $\alpha(1\rightarrow6)$  H-1), 4.98 (bs, H-1 $^{\text{s}}$ ), 4.63 (d,  $^3J_{1,2} = 7.2$  Hz,  $\beta$  reducing end H-1), 4.02-  
231 3.93 (m, H-3,6 $^{\text{a}}$ ,  $\text{CH}_2\text{C}\equiv$ ), 3.78-3.73 (m, H-5,6 $^{\text{b}}$ ), 3.60 (dd,  $^3J_{1,2} = 3.0$  Hz,  $^3J_{2,3} = 9.7$  Hz, H-2), 3.55 (t,  $^3J = 9.4$   
232 Hz, H-4), 3.51 (t,  $^3J = 9.9$  Hz, H-4 $^{\text{s}}$ ), 3.44 (t,  $^3J = 9.5$  Hz, H-4 $^{\text{s}}$ ), 3.03 (bs,  $\equiv\text{CH}$ ), 2.95 (bs,  $\equiv\text{CH}$ ), 2.69 (app  
233 bd,  $J_{\text{app}} = 8.7$  Hz,  $\equiv\text{CH}$ );  $^{13}\text{C}$  NMR (150 MHz,  $\text{D}_2\text{O}$ )  $\delta$  (ppm): 157.9 (CO), 157.0 (CO), 99.3, 98.2, 97.7  
234 ( $\alpha(1\rightarrow6)$  C-1), 95.6 (C-1 $^{\text{s}}$ ), 80.4-78.8 (C $\equiv$ ), 76.7, 73.4 (C-3), 73.2-73.1 ( $\equiv\text{CH}$ ), 72.0, 71.4 (C-2), 71.0, 70.2 (C-

235 5), 69.9, 69.5 (C-4), 67.7, 65.5 (C-6), 65.2, 60.5, 30.1 (CH<sub>2</sub>C≡); Anal. found C 40.90%, H 6.536%, N 1.42%.  
236 The number average molecular weight and the molar-mass dispersity were measured to be  $M_n$  =  
237 35,240 g/mol and  $\bar{D}$  = 1.14, respectively.

238 **2.2.6. Synthesis of DEX-ALN<sub>75</sub>-PEG<sub>25</sub> (6):** Pre-dried LiCl (90 mg, 2.123 mmol) and DEX-PC 5 (350  
239 mg, 0.0079 mmol containing 0.397 mmol of propargyl groups) were dissolved in H<sub>2</sub>O (5 mL) and  
240 heated at 60°C. A solution of sodium alendronate derivative 3 (127 mg, 0.298 mmol) in H<sub>2</sub>O (2 mL)  
241 was added, followed by a suspension of CuSO<sub>4</sub> (29 mg, 0.179 mmol) and sodium ascorbate (118 mg,  
242 0.596 mmol) in H<sub>2</sub>O (1 mL), and the mixture was stirred at 90°C overnight. After cooling down to  
243 room temperature, azide 4 (809 mg, 0.397 mmol) and a suspension of CuSO<sub>4</sub> (38 mg, 0.238 mmol) and  
244 sodium ascorbate (157 mg, 0.794 mmol) in H<sub>2</sub>O (0.8 mL) were subsequently added. The mixture was  
245 stirred for 22 h at 90 °C, then diluted with H<sub>2</sub>O (10 mL), filtered through filtering paper and then  
246 through a 0.45 μm syringe filter. Aqueous 0.1 M NaOH was added until pH ~7.0, followed by a  
247 solution of 10 mM EDTA at pH 7.0 (20 mL). The pH was then monitored and kept at ~7.0 with 0.1 M  
248 NaOH for 24 h. The mixture was again filtered through 0.45 μm syringe filter, lyophilized, re-  
249 dissolved in the minimum amount of water and dialyzed (12000-14000 Da MWCO) against distilled  
250 water, changing dialysate solution each 3 hours until its conductivity was stable and below 1 μS/cm  
251 (3 days for final value of 0.60 μS/cm) to yield DEX-ALN<sub>75</sub>-PEG<sub>25</sub> 7 (881 mg) as a brownish solid after  
252 lyophilization: FT-IR (KBr)  $\nu/\text{cm}^{-1}$ : 3423, 2913, 2880, 1645, 1457, 1352, 1298, 1252, 1104, 1041, 952, 845,  
253 548; <sup>1</sup>H NMR (600 MHz, D<sub>2</sub>O)  $\delta$  (ppm): 8.03 (bs, H-5-C<sub>2</sub>HN<sub>3</sub>), 5.35 (bs,  $\alpha$ (1→3,4) H-1), 5.27 (bs,  $\alpha$   
254 reducing end H-1), 5.18 (app t,  $J_{\text{app}}$  = 5.0 Hz, CH-OCONH), 5.04 (bs, H-1<sup>s</sup>), 5.00 (bs,  $\alpha$ (1→6) H-1), 4.64  
255 (bs,  $\beta$  reducing end H-1), 4.51-4.44 (m, OCH<sub>2</sub>CH<sub>2</sub>-C<sub>2</sub>HN<sub>3</sub>), 4.40-4.38 (m, CH<sub>2</sub>-C<sub>2</sub>HN<sub>3</sub>), 4.31-4.28 (m,  
256 NHCH<sub>2</sub>-C<sub>2</sub>HN<sub>3</sub>), 4.02-3.93 (m, H-5,6<sup>a</sup>), 3.87-3.84 (m,  $^1J_{\text{H,C}}$  = 140.2 Hz, <sup>13</sup>C satellite peak), 3.73 (bs, H-3,6<sup>b</sup>,  
257 OCH<sub>2</sub>CH<sub>2</sub>O), 3.67-3.64 (m, OCH<sub>2</sub>CH<sub>2</sub>-C<sub>2</sub>HN<sub>3</sub>), 3.61-3.60 (m, H-2), 3.56-3.52 (m, H-4), 3.45 (app t,  $J_{\text{app}}$  =  
258 9.3 Hz, H-4<sup>s</sup>), 3.40 (s, CH<sub>3</sub>O), 3.34-3.19 (CH<sub>2</sub>NH), 2.88 (bs, ≡CH), 2.78 (bs, ≡CH), 2.64 (bs, ≡CH), 2.23  
259 (bs, CH<sub>2</sub>CO), 1.93 (bs, CH<sub>2</sub>C), 1.77 (bs, CH<sub>2</sub>CH<sub>2</sub>C), 1.61 (CH<sub>2</sub>CH<sub>2</sub>CO, CH<sub>2</sub>CH<sub>2</sub>-C<sub>2</sub>HN<sub>3</sub>), 1.30-1.16 (bs,  
260 CH<sub>2</sub>CH<sub>2</sub>CH<sub>2</sub>CO); <sup>31</sup>P NMR (242.9 MHz, D<sub>2</sub>O)  $\delta$  (ppm): -1.4(-2.6) (C(PO<sub>3</sub>)<sub>2</sub>); Anal.: found C 46.24%, H  
261 7.582%, N 2.46%. HR-ICP-MS: found P 0.81%, Na 0.103%, Cu 1.05%, Li 0.042%.

262 **2.2.7. Synthesis of DEX-ALN<sub>50</sub>-PEG<sub>50</sub> (7):** Pre-dried LiCl (90 mg, 2.123 mmol) and DEX-PC 5 (350  
263 mg, 0.0079 mmol containing 0.397 mmol of propargyl groups) were dissolved in H<sub>2</sub>O (5 mL) and  
264 heated at 60°C. A solution of sodium alendronate derivative 3 (85 mg, 0.198 mmol) in H<sub>2</sub>O (1.5 mL)  
265 was added, followed by a suspension of CuSO<sub>4</sub> (19 mg, 0.119 mmol) and sodium ascorbate (79 mg,  
266 0.397 mmol) in H<sub>2</sub>O (1 mL), and the mixture was stirred at 90°C overnight. After cooling down to  
267 room temperature, azide 4 (809 mg, 0.397 mmol) and a suspension of CuSO<sub>4</sub> (38 mg, 0.238 mmol) and  
268 sodium ascorbate (157 mg, 0.794 mmol) in H<sub>2</sub>O (0.8 mL) were subsequently added. The mixture was  
269 stirred for 22 h at 90 °C, then diluted with H<sub>2</sub>O (10 mL), filtered through filtering paper and then  
270 through a 0.45 μm syringe filter. Aqueous 0.1 M NaOH was added until pH ~7.0, followed by a  
271 solution of 10 mM EDTA at pH 7.0 (20 mL). The pH was then monitored and kept at ~7.0 with 0.1 M  
272 NaOH for 24 h. The mixture was again filtered through 0.45 μm syringe filter, lyophilized, re-  
273 dissolved in the minimum amount of water and dialyzed (12000-14000 Da MWCO) against distilled  
274 water, changing dialysate solution each 3 hours until its conductivity was stable and below 1 μS/cm  
275 (3 days for final value of 0.74 μS/cm) to yield DEX-ALN<sub>50</sub>-PEG<sub>50</sub> 6 (928 mg) as a brownish solid after  
276 lyophilization: FT-IR (KBr)  $\nu/\text{cm}^{-1}$ : 3429, 2917, 2881, 1645, 1457, 1352, 1253, 1103, 952, 558; <sup>1</sup>H NMR  
277 (600 MHz, D<sub>2</sub>O)  $\delta$  (ppm): 8.03 (bs, H-5-C<sub>2</sub>HN<sub>3</sub>), 5.35 (bs,  $\alpha$ (1→3,4) H-1), 5.26 (bs,  $\alpha$  reducing end H-  
278 1), 5.18 (app t,  $J_{\text{app}}$  = 5.0 Hz, CH-OCONH), 5.04 (bs, H-1<sup>s</sup>), 5.00 (bs,  $\alpha$ (1→6) H-1), 4.64 (bs,  $\beta$  reducing  
279 end H-1), 4.47-4.43 (m, OCH<sub>2</sub>CH<sub>2</sub>-C<sub>2</sub>HN<sub>3</sub>), 4.40-4.38 (m, CH<sub>2</sub>-C<sub>2</sub>HN<sub>3</sub>), 4.31-4.29 (m, NHCH<sub>2</sub>-C<sub>2</sub>HN<sub>3</sub>),  
280 4.02-3.93 (m, H-5,6<sup>a</sup>), 3.87-3.84 (m,  $^1J_{\text{H,C}}$  = 140.4 Hz, <sup>13</sup>C satellite peak), 3.73 (bs, H-3,6<sup>b</sup>, OCH<sub>2</sub>CH<sub>2</sub>O),  
281 3.67-3.64 (m, OCH<sub>2</sub>CH<sub>2</sub>-C<sub>2</sub>HN<sub>3</sub>), 3.61-3.59 (m, H-2), 3.56-3.52 (m, H-4), 3.43 (app t,  $J_{\text{app}}$  = 10.0 Hz, H-  
282 4<sup>s</sup>), 3.41 (s, CH<sub>3</sub>O), 3.32-3.18 (CH<sub>2</sub>NH), 2.88 (bs, ≡CH), 2.70 (bs, ≡CH), 2.25 (bs, CH<sub>2</sub>CO), 1.93 (bs,  
283 CH<sub>2</sub>C), 1.78 (bs, CH<sub>2</sub>CH<sub>2</sub>C), 1.61 (CH<sub>2</sub>CH<sub>2</sub>CO, CH<sub>2</sub>CH<sub>2</sub>-C<sub>2</sub>HN<sub>3</sub>), 1.26 (bs, CH<sub>2</sub>CH<sub>2</sub>CH<sub>2</sub>CO); <sup>31</sup>P NMR  
284 (242.9 MHz, D<sub>2</sub>O)  $\delta$  (ppm): -1.8(-2.9) (C(PO<sub>3</sub>)<sub>2</sub>); Anal.: found C 46.85%, H 7.769%, N 2.27%. HR-ICP-

285 MS: found P 0.57%, Na 0.060%, Cu 0.74%, Li 0.027%. The number average molecular weight and the  
286 molar-mass dispersity were measured to be  $M_n = 83,120$  g/mol and  $\bar{D} = 1.36$ , respectively.

287 **2.2.8. Synthesis of DEX-ALN<sub>25</sub>-PEG<sub>75</sub> (8):** Pre-dried LiCl (90 mg, 2.123 mmol) and DEX-PC 5 (350  
288 mg, 0.0079 mmol containing 0.397 mmol of propargyl groups) were dissolved in H<sub>2</sub>O (5 mL) and  
289 heated at 60°C. A solution of sodium alendronate derivative 3 (43 mg, 0.100 mmol) in H<sub>2</sub>O (1 mL)  
290 was added, followed by a suspension of CuSO<sub>4</sub> (10 mg, 0.060 mmol) and sodium ascorbate (40 mg,  
291 0.200 mmol) in H<sub>2</sub>O (1 mL), and the mixture was stirred at 90°C overnight. After cooling down to  
292 room temperature, azide 4 (809 mg, 0.397 mmol) and a suspension of CuSO<sub>4</sub> (38 mg, 0.238 mmol) and  
293 sodium ascorbate (157 mg, 0.794 mmol) in H<sub>2</sub>O (0.8 mL) were subsequently added. The mixture was  
294 stirred for 22 h at 90 °C, then diluted with H<sub>2</sub>O (10 mL), filtered through filtering paper and then  
295 through a 0.45 μm syringe filter. Aqueous 0.1 M NaOH was added until pH ~7.0, followed by a  
296 solution of 10 mM EDTA at pH 7.0 (20 mL). pH was then monitored and kept at ~7.0 with 0.1 M  
297 NaOH for 24 h. The mixture was again filtered through 0.45 μm syringe filter, lyophilized, re-  
298 dissolved in the minimum amount of water and dialyzed (12000-14000 Da MWCO) against distilled  
299 water, changing dialysate solution each 3 hours until its conductivity was stable and below 1 μS/cm  
300 (2 days for final value of 0.63 μS/cm) to yield DEX-ALN<sub>25</sub>-PEG<sub>75</sub> 8 (978 mg) as a brownish solid after  
301 lyophilization: FT-IR (KBr) v/cm<sup>-1</sup>: 3423, 2912, 2880, 1645, 1457, 1352, 1299, 1253, 1104, 1042, 1019, 951,  
302 845, 550; <sup>1</sup>H NMR (600 MHz, D<sub>2</sub>O) δ (ppm): 8.03 (bs, H-5-C<sub>2</sub>H<sub>N</sub><sub>3</sub>), 5.35 (bs, α(1→3,4) H-1), 5.27 (bs, α  
303 reducing end H-1), 5.19 (app t,  $J_{app} = 5.0$  Hz, CH-OC(=O)NH), 5.05 (bs, H-1<sup>s</sup>), 5.00 (bs, α(1→6) H-1), 4.90  
304 (bs, H-1<sup>s</sup>), 4.64 (bs, β reducing end H-1), 4.64 (bs, OCH<sub>2</sub>CH<sub>2</sub>-C<sub>2</sub>H<sub>N</sub><sub>3</sub>), 4.40-4.38 (m, CH<sub>2</sub>-C<sub>2</sub>H<sub>N</sub><sub>3</sub>), 4.31-  
305 4.28 (m, NHCH<sub>2</sub>-C<sub>2</sub>H<sub>N</sub><sub>3</sub>), 4.02-3.93 (m, H-5,6<sup>a</sup>), 3.85-3.84 (m,  $^1J_{H,C} = 140.4$  Hz, <sup>13</sup>C satellite peak), 3.73  
306 (bs, H-3,6<sup>b</sup>, OCH<sub>2</sub>CH<sub>2</sub>O), 3.68-3.64 (m, OCH<sub>2</sub>CH<sub>2</sub>-C<sub>2</sub>H<sub>N</sub><sub>3</sub>), 3.61-3.59 (m, H-2), 3.56-3.52 (m, H-4), 3.45  
307 (app t,  $J_{app} = 9.6$  Hz, H-4<sup>s</sup>), 3.41 (s, CH<sub>3</sub>O), 3.32-3.19 (CH<sub>2</sub>NH), 3.02 (bs, ≡CH), 2.95 (bs, ≡CH), 2.23 (bs,  
308 CH<sub>2</sub>CO), 1.93 (bs, CH<sub>2</sub>C), 1.78 (bs, CH<sub>2</sub>CH<sub>2</sub>C), 1.61 (CH<sub>2</sub>CH<sub>2</sub>CO, CH<sub>2</sub>CH<sub>2</sub>-C<sub>2</sub>H<sub>N</sub><sub>3</sub>), 1.31-1.22 (bs,  
309 CH<sub>2</sub>CH<sub>2</sub>CH<sub>2</sub>CO); <sup>31</sup>P NMR (242.9 MHz, D<sub>2</sub>O) δ (ppm): 0.5-0.1, -1.5-(-2.4) (C(PO<sub>3</sub>)<sub>2</sub>); Anal.: found C  
310 47.86%, H 7.842%, N 2.05%. HR-ICP-MS: found P 0.26%, Na 0.092%, Cu 0.42%, Li 0.048%.

### 311 2.3 Synthesis and characterization of MIL-100(Fe) nanoMOFs

312 Iron trimesate nanoMOFs were synthesized using a microwave-assisted hydrothermal method  
313 as previously described [6]. Briefly, 30 mL of an aqueous mixture containing 6.0 mM iron chloride  
314 hexahydrate and 4.0 mM of 1,3,5-benzenetricarboxylic acid was heated at 130 °C under stirring prior  
315 to microwave irradiation at 1600 W (Mars-5, CEM, USA). The synthesized nanoMOFs were recovered  
316 by centrifugation at 10000 g for 15 min and purified by washing six times with absolute ethanol. Their  
317 morphology was observed with a transmission electron microscope (TEM, JEOL 1400 (120 kV),  
318 Japan). Mean hydrodynamic diameters and size distributions were determined by dynamic light  
319 scattering (DLS, Malvern Nano-ZS, Zetasizer Nano series, France). NanoMOFs' Zeta potential (ZP)  
320 was measured at 25 °C using a Zetasizer Nano-ZS instrument in a pH range of 1 to 10. For this,  
321 nanoMOFs were diluted to a final concentration of 100 μg/mL using a 1 mM KCl solution. The  
322 nanoMOF specific surface area was measured by nitrogen sorption experiments at -196 °C on an  
323 ASAP 2020 (Micromeritics, USA) after sample degassing at 100 °C for 15 h under high vacuum. X-  
324 ray powder diffraction patterns (XRPD) were recorded for crystallinity characterization. NanoMOFs  
325 were stored in ethanol at room temperature and re-suspended in aqueous media whenever needed.

### 326 2.4 Surface modification of MIL-100(Fe) nanoMOFs and their characterization

#### 327 2.4.1 Preparation and characterization of DEX-ALN-PEG coated nanoMOF

328 NanoMOFs were centrifuged at 10000 g for 10 min to remove the storage solvent (ethanol) and  
329 then re-dispersed in water by vortex. For coating, they were incubated overnight at room temperature  
330 with DEX-ALN-PEG solutions at mass ratios DEX-ALN-PEG: nanoMOFs of 1:4, 1:2 and 1:1. The non-  
331 attached DEX-ALN-PEG fraction was removed by centrifugation (10000 g, 10 min). The pellets were

332 dried and the adsorbed DEX-ALN-PEG was quantified by inductively coupled plasma mass  
333 spectrometry (ICP-MS). Briefly, nanoMOFs before and after modification with DEX-ALN-PEG were  
334 digested using *aqua regia* (15 minutes under ultrasonic bath), and phosphorous (P) quantification was  
335 performed using an ICP-MS equipped with a triple quadrupole (Agilent 8800, Agilent Technologies,  
336 Japan). Operation conditions were daily optimized using a tuning solution. P isotope was detected  
337 using “mass shift mode” ( $^{47}\text{PO}^+$ ) after reaction with oxygen in the cell. Conversely, scandium (Sc)  
338 (added as internal standard on samples and calibration standards solutions at a concentration of 10  
339  $\mu\text{g/L}$ ) was detected on “mass mode” ( $^{45}\text{Sc}^+$ ). Oxygen was introduced into the collision/reaction cell at  
340 a flow rate of 0.35 mL/min. Dwell time for each of the targeted isotopes was 1 s. P was quantified  
341 using external calibration using certified 1000 mg/L P standard solution (Merck, Germany).

342 The amount A of DEX-ALN-PEG associated to nanoMOFs was calculated on the basis of their P  
343 content by the following formula:

$$344 \quad A = \frac{P1}{P2} 100\%$$

345 where (P1 wt%) is the phosphorous content in the coated nanoMOFs and (P2 wt%) is the  
346 phosphorous content in the synthesized DEX-ALN-PEG copolymers.

347 DEX-ALN-PEG coated nanoMOF were characterized in the same fashion as the uncoated  
348 samples to determine their size distribution, morphology and surface charge. The crystallinity of  
349 DEX-ALN-PEG coated nanoMOF was characterized by XRPD.

#### 350 2.4.2 Colloidal stability investigation

351 Colloidal stabilities of DEX-ALN-PEG coated nanoMOFs were estimated by DLS after  
352 incubation in both MilliQ water and cell culture medium (DMEM complemented with 10% FBS, 1%  
353 penicillin/streptomycin (100 mg/mL) and 1% L-glutamine). Mean hydrodynamic diameters were  
354 measured at 6 h, 1, 2, 4, 7, 9, 14, 18 and 21 d storage at 4 °C in water, and at 0, 2, 4, 6, and 8 h after  
355 incubation at 37 °C in cell culture media.

#### 356 2.4.3 Human albumin adsorption studies

357 NanoMOFs coated or not with DEX-ALN-PEG (300  $\mu\text{g/mL}$ ) were incubated with HSA solutions  
358 at 100  $\mu\text{g/mL}$  in 10 mM phosphate buffer (PB) at 37 °C. The samples were centrifuged at 10000 g for  
359 5 min to recover the nanoMOF pellets after 1, 2, 3, 4, 6, 8 and 12 h incubation. The excessive HSA in  
360 the supernatant was quantified using a bicinchoninic acid (BCA) assay.

#### 361 2.4.4 “Stealth” effect of the DEX-ALN-PEG shell

362 **Visualization by optical microscopy.** A direct visualization of the MIL-100(Fe) nanoMOFs  
363 inside J774A.1 macrophages was achieved based on iron staining using a Prussian blue staining kit.  
364 In a 24-well plate (with cover slips)  $1 \times 10^5$  J774A.1 macrophages were placed with RPMI complete  
365 medium and 10% FBS. Each well of macrophages was treated with 50  $\mu\text{g}$  of nanoMOFs, either coated  
366 or not with DEX-ALN-PEG. The macrophages were subsequently incubated for 2 and 4 h in an  
367 incubator at 37 °C with a  $\text{CO}_2$  concentration of 5%. Afterwards the wells were washed with complete  
368 medium and then further washed twice with PBS. Cells were fixed with 4% paraformaldehyde,  
369 washed and incubated for 10 minutes with 2% potassium ferrocyanide in 0.6 mM hydrochloric acid.  
370 Cells were washed again with PBS, counterstained with pararosaniline hydrochloride (0.02%) and  
371 placed on a glass slide. A drop of emersion oil was applied to each coverslip and evaluated for iron  
372 staining using light microscopy.

373 **Fe quantification by ICP-MS.** Macrophage cells (J774A.1) were seeded overnight at a density of  
374  $3.0 \times 10^5$  cells per well in 24-well plates in cell culture medium at 37°C in 5%  $\text{CO}_2$ . Cells were then  
375 incubated with 1 mL cell culture media containing nanoMOFs coated or not with DEX-ALN-PEG for  
376 2, 4 and 6 h (nanoMOFs concentration = 50  $\mu\text{g/mL}$ ). At the end of the incubation, the cells were



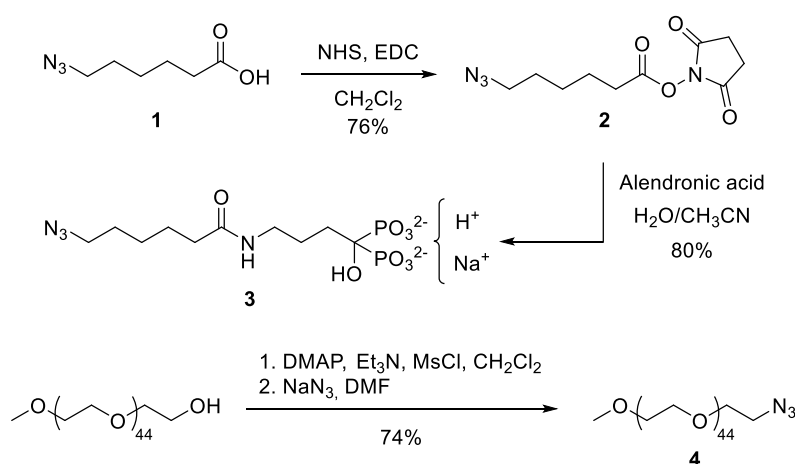
377 washed with PBS for three times to eliminate the nanoMOFs which did not interact with the cells.  
 378 Cells were finally dried and digested using *aqua regia* (15 minutes under ultrasonic bath). Fe  
 379 quantification was performed using an ICP-MS equipped with a triple quadrupole (Agilent 8800).  
 380 Operation conditions were daily optimized using a tuning solution. Fe and Co (added as internal  
 381 standard on samples and calibration standards solution at a concentration of 10  $\mu\text{g/L}$ ) isotopes were  
 382 detected using "on-mass mode" ( $^{54}\text{Fe}^+$ ,  $^{56}\text{Fe}^+$ ,  $^{59}\text{Co}^+$ ). Helium was introduced into the collision/reaction  
 383 cell at a flow rate of 3  $\text{mL min}^{-1}$ . Dwell time for each of the targeted isotopes was 1 s. Fe was quantified  
 384 using external calibration prepared using certified 1000  $\text{mg/L}$  Fe standard solution (Merck,  
 385 Germany).

### 386 3. Results and discussion

#### 387 3.1. Synthesis and characterization of DEX-ALN-PEG copolymers

388 For the post-synthetic modification of the surface of MIL-100(Fe) MOF nanoparticles we planned to  
 389 prepare DEX derivatives appended with alendronate (ALN) moieties and PEG chains. For this  
 390 strategy, we first prepared alendronate and PEG azide derivatives **3** and **4**, respectively (Scheme 1).  
 391 We then appended them on dextran T-40 grafted with a controlled number of terminal alkyne  
 392 residues in the form of propargyl carbamate groups (DEX-PC **5**) (Scheme 2) through a Cu(I)-catalyzed  
 393 azide-alkyne cycloaddition (CuAAC) reaction to yield DEX-ALN-PEG conjugates **6-8**.

394



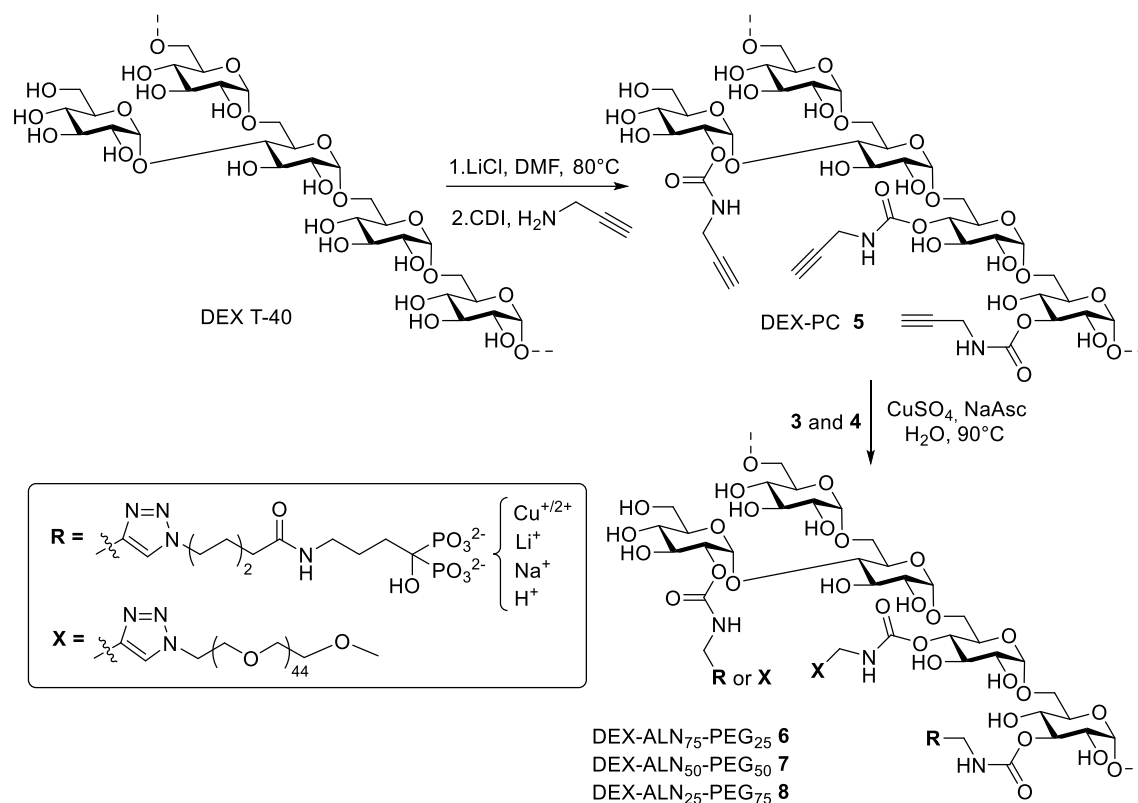
395

#### 396 Scheme 1. Synthesis of azide derivatives **3** and **4**.

397 First, we synthesized azide alendronate derivative **3** (Scheme 1). The reaction between NHS-ester **2**  
 398 and alendronate monosodium salt was performed in a  $\text{MeCN:H}_2\text{O}$  mixture keeping the pH at  $\sim 8.5$   
 399 in order both to ensure the solubility of the alendronate salt and to guarantee the nucleophilic  
 400 properties of the primary amine. However, precipitation of the crude after solvent evaporation with  
 401  $\text{EtOH}$  afforded product **3** with *N*-hydroxysuccinimide (NHS) byproduct, as confirmed by  $^1\text{H}$  NMR  
 402 spectra. Attempts to remove NHS by solid-liquid extraction using organic solvents, including  $\text{EtOAc}$   
 403 and  $\text{CH}_3\text{CN}$ , failed. Thus, compound **3** was finally isolated by column chromatography using 5:1  
 404  $\text{CH}_3\text{CN:H}_2\text{O}$  as initial eluent until NHS was washed out of the column, and 2:1  $\text{CH}_3\text{CN:H}_2\text{O}$  for  
 405 eluting pure **3** in 80% yield after lyophilization. In the initial alkaline pH  $\sim 8.5$  environment, product  
 406 **3** should be most likely in a trisodium salt form [26]. However, flash column chromatography  
 407 probably changed the distribution curves of the species in equilibrium by partial acidification of the  
 408 mixture. Indeed, negative ESI-TOF mass spectrum depicted the species  $[\text{M} - \text{Na}]^-$  and  $[\text{M} - \text{H}]^-$ ;  
 409 considering  $\text{M}$  as the monosodium salt. Similarly, positive ESI-TOF mass spectrum showed  $[\text{M} + \text{H}]^+$ ,

410  $[M + Na]^+$ ,  $[M - H + 2Na]^+$  and  $[M - 2H + 3Na]^+$ , suggesting that the alendronate derivative was  
 411 obtained mainly as the monosodium salt species.

412 Synthesis of azido PEG chain **4** was performed in two sequential steps. First, commercial  
 413 MeOPEG<sub>45</sub>OH, having a methoxy group at one end of the chain, was mesylated and used without  
 414 any further purification for the reaction with sodium azide in DMF. Azido PEG **4** was isolated by two  
 415 subsequent filtration processes with THF and Et<sub>2</sub>O that yielded **4** pure enough, as confirmed by NMR  
 416 analysis. It is important to remark that the broad signal observed at  $\delta$  3.65-3.61 ppm corresponding  
 417 to the main chain methylene groups appeared along with <sup>13</sup>C satellites due to the <sup>13</sup>C-<sup>1</sup>H coupling  
 418 typically observed in high molecular weight PEG derivatives [27].



437 different positions on the glucose moieties. In addition, a set of new signals arose from the substituted  
438 glucose units, namely a doublet at  $\delta$  5.06 ppm and broad singlet  $\delta$  4.98 ppm corresponding to  
439 anomeric protons, along with two triplets at  $\delta$  3.51 and 3.44 ppm assigned to the H-4 protons. In  $^{13}\text{C}$   
440 NMR spectrum, signals at  $\delta$  157.9-157.0 ppm indicated the presence of carbonyl groups on the  
441 structure, while the quaternary and ternary carbons of the ethynyl group gave peaks in the range of  
442  $\delta$  80.4-78.8 and  $\delta$  73.2-73.1 ppm, respectively.

443 Once DEX-PC 5 was prepared, azides 3 and 4 were conjugated using  $\text{CuSO}_4$  and sodium ascorbate  
444 as catalyst system at  $90^\circ\text{C}$  in water (Scheme 2). Three dextran derivatives with different ratios of ALN  
445 and PEG branches were prepared, namely DEX-ALN<sub>75</sub>-PEG<sub>25</sub> 6, DEX-ALN<sub>50</sub>-PEG<sub>50</sub> 7 and DEX-ALN<sub>25</sub>-  
446 PEG<sub>75</sub> 8, in order to study the effect of such ratio on both the stability of the coating and the “stealth”  
447 abilities of the resulting surface-modified nanoMOFs. To prevent that different diffusion coefficients  
448 and reactivity kinetics of structurally so different azides as 3 and 4 might condition the actual ratio  
449 on 6-8, conjugations were performed sequentially starting with the required amount of alendronate  
450 derivative 3, followed after 8 hours by addition of an excess of PEG azide 4. It was expected that the  
451 conjugation of the short chain of alendronate in the first place would not hinder the subsequent  
452 approach of the much bulkier PEG chain in the second step, which might occur if performed in the  
453 opposite order. Purification of 6-8 was carried out by washing with a solution of EDTA at pH ~7 in  
454 order to chelate the excess of copper, followed by dialysis against water using 12-14 KDa MWCO  
455 membranes until stable conductivity ( $<1\ \mu\text{S}/\text{cm}$ ) was obtained in the dialysate solution. The analysis  
456 of number average molecular weights ( $M_n$ ) of polymers before (DEX-PC 5) and after (DEX-ALN<sub>50</sub>-  
457 PEG<sub>50</sub> 7) chemical modification by PEG chains was achieved by SEC-MALLS. The starting material,  
458 DEX had a  $M_n$  value of 31,150 g/mol. It was further shown that grafting ALN and PEG resulted in an  
459 expected increase of number average molecular weight with the grafting of PEG chains on the main  
460 DEX chain (from 35,240 for DEX-PC 5 to 83,120 g/mol for DEX-ALN<sub>50</sub>-PEG<sub>50</sub> 7). This difference of  
461 around 50,000 g/mol could correspond to a ratio of 25% of PEG grafted chains of 2000 g/mol (since  
462  $50\% \times 2000\ \text{g/mol} \times 100\ \text{units} = 100,000\ \text{g/mol}$ ). Nevertheless, note that this determination presents a  
463 high uncertainty notably due to the hypothesis that the refractive index increment value of DEX-  
464 ALN<sub>50</sub>-PEG<sub>50</sub> was equal to the one of unmodified dextran ( $dn/dc = 0.147\ \text{ml/g}$ ). Consequently,  
465 elemental analysis and HR-ICP-MS of the obtained copolymers was carried out in order to obtain a  
466 more accurate compositional profile for DEX-ALN-PEG derivatives 6-8. The mathematical model  
467 constructed to analyze these data (see supplementary material) indicated that only 66-74% of  
468 propargyl carbamates underwent cycloaddition (Table 1). Interestingly, the average number of ALN  
469 branches appended to the polysaccharide consistently changed depending on the initial ratio of  
470 reagents although in lesser extension than foreseen, varying from ~15 in the case of DEX-ALN<sub>75</sub>-PEG<sub>25</sub>  
471 6 to ~5 for DEX-ALN<sub>25</sub>-PEG<sub>75</sub> 8. In sharp contrast, the average number of PEG branches only varies  
472 from ~26 in the case of PEG-ALN<sub>75</sub>-PEG<sub>25</sub> 6 and ~32 for DEX-ALN<sub>25</sub>-PEG<sub>75</sub> 8. This fact suggests that  
473 cycloaddition of PEG azide derivative 4 onto DEX-PC 5 is mainly limited by steric hindrance of the  
474 resulting product more than the reagent amount added to the reaction. The robustness of the model  
475 is evidenced by the fact that the sum of free propargyl carbamate ( $n$ ), ALN ( $x$ ) and PEG ( $z$ ) branches  
476 keeps around 50 ( $\pm 12\%$ ), which matches the estimated number of propargyl carbamate groups  
477 originally present in DEX-PC 5 starting material. It should be underlined that the model predicts the  
478 presence of at least one Cu atom per alendronate branch, along with an extra cation of Na and/or Li,  
479 even after extraction with EDTA prior dialysis. This result is not surprising since it is known that  
480 alendronate can chelate Cu(II) in a wide range of pH [29,30], and indeed may explain the reduced  
481 cycloaddition efficiency for alendronate branches since copper cations could have been sequestered  
482 during the reaction. Although free, unbound Cu(II) has been demonstrated to be toxic for living cells  
483 [31], it requires concentrations as high as  $78.5\ \mu\text{mol/L}$  (5 mg/L) in serum for systemic toxicity in  
484 humans [32]. Furthermore, the toxicity of chelated copper is remarkably lower, allowing its use to  
485 perform CuAAC reactions within living systems [33,34]. We observed that copper present in DEX-  
486 ALN-PEG 6-8 did not hinder MIL-100(Fe) coating (see below) which took place through their  
487 alendronate branches, and most likely, it was displaced by iron(III) atoms from nanoMOFs surface

488 and washed out during centrifugation isolation. The proposed structures for 6-8 were demonstrated  
 489 by  $^1\text{H}$  NMR spectra, where the formation of 1,2,3-triazole residues caused the appearance of a broad  
 490 signal at  $\delta$  8.03 ppm in the three cases. In addition, methylene protons of PEG residues gave an intense  
 491 peak at  $\delta$  3.73 ppm, while weak and broad singlets observed between  $\delta$  2.25 and 1.26 ppm evidenced  
 492 the presence of alendronate branches. Furthermore, signals from non-reacted ethynyl protons were  
 493 still notorious between  $\delta$  3.02 and 2.64 ppm, as the compositional model had predicted (Table 1).  $^{13}\text{C}$   
 494 NMR experiments were strongly dominated by the high signals arising from PEG methylenes, which  
 495 hindered both their acquisition and assignation. Finally,  $^{31}\text{P}$  NMR confirmed the presence of  
 496 phosphorus nuclei in the molecules with signals at  $\delta$  0.5-(-2.6) ppm.

497 **Table 1.** Calculated (see supplementary material) number of free propargyl carbamate ( $n$ ),  
 498 alendronate ( $x$ ) and PEG ( $z$ ) branches from compositional profiles obtained by elemental analyses  
 499 and HR-ICP-MS data.<sup>a</sup>

Derivative	$n$ <i>Nb of propargyl groups</i>	$x$ <i>Nb of alendronate</i>	$z$ <i>Nb of PEG chains</i>	$n+x+z$
DEX-PC 5	50.1	0	-0.1	50.1
DEX-ALN <sub>75</sub> -PEG <sub>25</sub> 6	16.1	14.3	26.0	56.4
DEX-ALN <sub>50</sub> -PEG <sub>50</sub> 7	13.7	10.8	30.5	55.0
DEX-ALN <sub>25</sub> -PEG <sub>75</sub> 8	17.6	4.9	32.3	54.8

500 <sup>a</sup>An error of  $\pm 12\%$  was estimated.

501

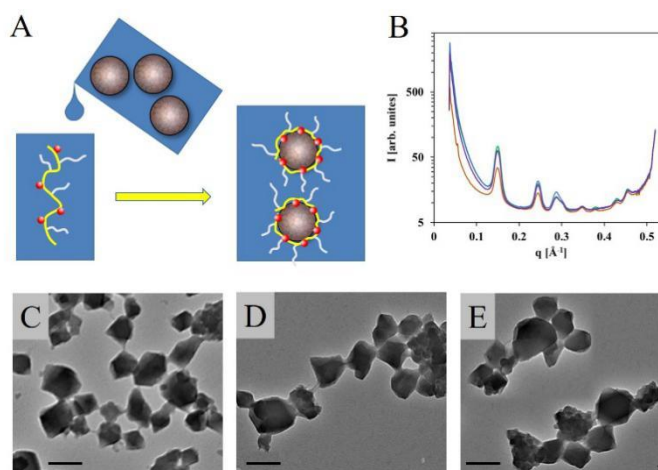
### 502 3.2. MIL-100(Fe) nanoMOFs synthesis and surface modification

#### 503 3.2.1 DEX-ALN-PEG coating and physicochemical characterization

504 MIL-100(Fe) nanoMOFs with a mean hydrodynamic diameter of  $191 \pm 23$  nm and BET (Brunauer,  
 505 Emmett and Teller) surface area of  $1690 \pm 80$  m<sup>2</sup> g<sup>-1</sup> were successfully synthesized by an organic  
 506 solvent-free microwave-assisted hydrothermal method. They exhibited a faceted morphology  
 507 (Figure 1C), crystalline structure (Figure 1B) and composition in agreement with previously reported  
 508 data [6,12].

509 Surface modification of MIL-100(Fe) nanoMOFs with DEX-ALN-PEG was carried out through a  
 510 simple, "green" (meaning organic solvent-free) method consisting on simple impregnation of  
 511 nanoMOFs in aqueous solutions of the synthesized copolymers (Figure 1A). The three copolymers  
 512 with increased PEG contents, namely DEX-ALN<sub>75</sub>-PEG<sub>25</sub> 6, DEX-ALN<sub>50</sub>-PEG<sub>50</sub> 7, and DEX-ALN<sub>25</sub>-  
 513 PEG<sub>75</sub> 8 were used for the surface modification.

514



515

516

517 **Figure 1.** Preparation and characterization of nanoMOFs coated or not with DEX-PEG. **A:**  
 518 schematic representation of the «green» preparation of DEX-ALN-PEG coated nanoMOFs in water;  
 519 **B:** XRPD patterns of nanoMOFs coated or not with DEX-PEG (orange: nanoMOFs; blue: DEX-ALN<sub>50</sub>-  
 520 PEG<sub>50</sub> coated nanoMOFs; green: DEX-ALN<sub>25</sub>-PEG<sub>75</sub> coated nanoMOFs; purple: DEX-ALN<sub>75</sub>-PEG<sub>25</sub>  
 521 coated nanoMOFs); **C-E:** TEM images of uncoated nanoMOFs (**C**), DEX-ALN<sub>50</sub>-PEG<sub>50</sub> **7** coated  
 522 nanoMOFs (**D**) and DEX-ALN<sub>25</sub>-PEG<sub>75</sub> **8** coated nanoMOFs (**E**); scale bar (200 nm). The mass ratios  
 523 DEX-ALN-PEG: nanoMOFs were 1:1.

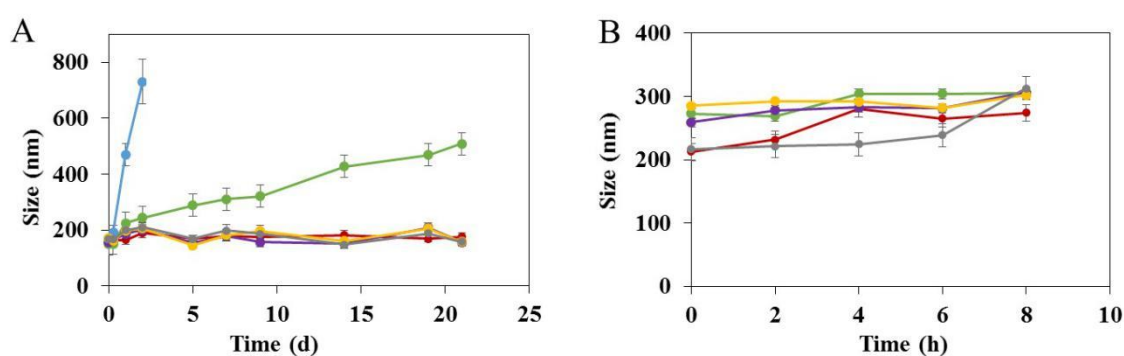
524 The amount of DEX-ALN-PEG associated to the nanoMOFs was determined by ICP-MS by  
 525 direct quantification of the P content in the coated samples. Indeed, P is the only element present in  
 526 the DEX-ALN-PEG copolymers, but not in the nanoMOFs, offering a straightforward and precise  
 527 quantification method. It was found that after overnight incubation, amounts of DEX-ALN<sub>75</sub>-PEG<sub>25</sub>  
 528 **6**, DEX-ALN<sub>50</sub>-PEG<sub>50</sub> **7**, and DEX-ALN<sub>25</sub>-PEG<sub>75</sub> **8** associated to the nanoMOFs reached  $29 \pm 2$  wt%,  
 529  $27 \pm 2$  wt% and  $32 \pm 3$  wt%, respectively. Interestingly, these amounts of coating material attached to the  
 530 nanoMOFs were among the highest reported so far. This efficient association could be possibly  
 531 attributed to: i) the strong affinity of ALN for iron site at the surface and ii) the cooperative effects of  
 532 ALN moieties as schematized in Figure 1A. As comparison, cyclodextrin (CD)-phosphate coatings  
 533 on same MIL-100(Fe) nanoMOFs reached  $\sim 17$  wt%. In that case, only 3-4 phosphate moieties were  
 534 attached to each CD [35]. Indeed, alendronate, used mainly for osteoporosis treatment, is known to  
 535 have a strong affinity for metals. It was incorporated in nanoMOFs made of Zr-based UiO-66 NPs  
 536 [36]. It was highlighted that this amino-bisphosphonate was probably strongly anchored to the Zr-O  
 537 clusters of the UiO NPs, thus promoting both high loading efficiencies (close to 100 %) and controlled  
 538 release.

539 These studies suggest that the amount of DEX-ALN-PEG associated to the nanoMOFs was not  
 540 significantly affected by the ratio of ALN used in the experiments. This suggest that a large number  
 541 of ALN moieties are not required for an efficient coating of the nanoMOFs, and that DXT-ALN<sub>25</sub>-  
 542 PEG<sub>75</sub> already shows enough ALN appendages ( $\sim 5$ ) to perform the most efficient coating we could  
 543 observed.

544 The MIL-100(Fe) nanoMOFs coated or not with DEX-ALN-PEG were characterized by a set of  
 545 complementary techniques. First, XRPD studies indicated that the crystalline structure of MIL-  
 546 100(Fe) nanoMOFs was preserved after surface modification (Figure 1B) in spite of the high amounts  
 547 of DEX-ALN-PEG associated to the nanoparticles. Second, TEM experiments showed that the  
 548 nanoMOFs maintained their faceted morphology, regardless of the type of DEX-ALN-PEG adsorbed  
 549 (Figures 1C-E).

550 The hydrodynamic diameters of MIL-100(Fe) nanoMOFs were determined by dynamic light  
 551 scattering (DLS) in water before and after surface modification. The mean hydrodynamic diameter  
 552 of nanoMOFs before coating was  $191 \pm 23$  nm. Whatever the amount and type of DEX-ALN-PEG  
 553 coating material, there were no significant mean size and polydispersity variations after the coating  
 554 process. Final mean diameters were in the range of  $193 \pm 21$  nm to  $209 \pm 31$  nm, indicating that the  
 555 coating thickness was less than 10 nm and that no aggregation occurred.

556 Uncoated nanoMOFs had a tendency to aggregate upon storage in water (Figure 2A), in  
 557 agreement with previous studies [12]. In contrast, nanoMOFs coated with all the DEX-ALN-PEG  
 558 samples (mass ratio DEX-ALN-PEG:nanoMOFs 1:1) were stable in water up to three weeks storage,  
 559 showing that their coating efficiently prevented their aggregation. However, the mass ratios DEX-  
 560 ALN-PEG:nanoMOFs play an important role on the colloid stability of the nanoMOFs. For example,  
 561 when reducing 4 fold the amount of DEX-ALN<sub>50</sub>-PEG<sub>50</sub> 7 at the nanoMOF surface (mass ratio DEX-  
 562 ALN-PEG:nanoMOFs 1:4), aggregation was observed during storage in water, as shown by a  
 563 diameter increase from 193 nm to more than 400 nm in 24 h (Figure 2A), possibly due to DEX-ALN-  
 564 PEG at the surface of nanoMOFs inducing a bridging effect. Therefore this sample was excluded in  
 565 the following experiments. All the nanoMOF formulations were stable in the biological medium used  
 566 in this study (DMEM complemented with 10% FBS) (Figure 2B). No aggregation was found and the  
 567 mean diameters remained constant over more than 6 h incubation at 37 °C, allowing for further  
 568 biological investigations of interactions with macrophages.



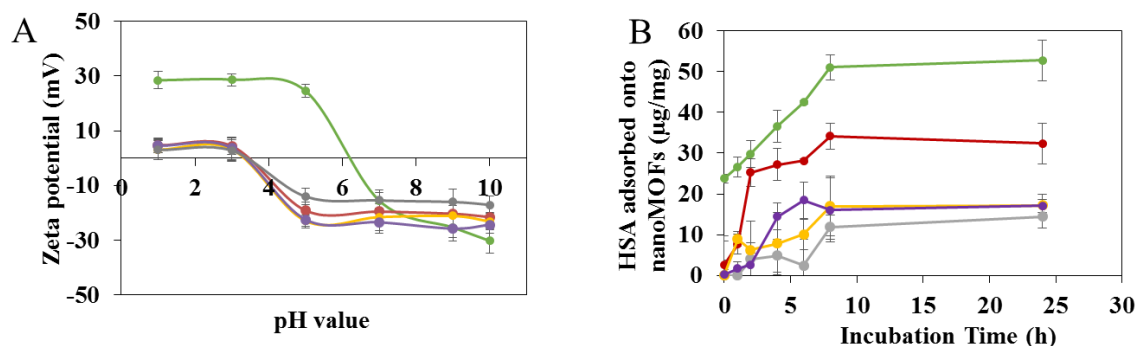
569

570 **Figure 2.** Stability of nanoMOFs coated or not with DEX-ALN-PEG in water (A) and in DMEM  
 571 cell culture medium (B). Blue: uncoated nanoMOF; purple: nanoMOF coated with DEX-ALN<sub>75</sub>-PEG<sub>25</sub>  
 572 6 (mass ratio DEX-ALN-PEG:nanoMOFs 1:1); orange: nanoMOF coated with DEX-ALN<sub>50</sub>-PEG<sub>50</sub> 7  
 573 (mass ratio DEX-ALN-PEG:nanoMOFs 1:1); gray: nanoMOF coated with DEX-ALN<sub>25</sub>-PEG<sub>75</sub> 8 (mass  
 574 ratio DEX-ALN-PEG:nanoMOFs 1:1); green: nanoMOF coated with DEX-ALN<sub>50</sub>-PEG<sub>50</sub> 7 (mass ratio  
 575 DEX-ALN-PEG:nanoMOFs 1:4); red: nanoMOF coated with DEX-ALN<sub>50</sub>-PEG<sub>50</sub> 7 (mass ratio DEX-  
 576 ALN-PEG: nanoMOFs 1:2).

### 577 3.2.2 Surface properties of nanoMOFs before and after functionalization

578 ZP measurements were performed to gain insights on the influence of the coatings on the global  
 579 charge of the NPs. The ZP of the nanoMOFs, coated or not, was found to be strongly dependent upon  
 580 the pH of the suspension medium, in a range of 1 to 10 (Figure 3A). Typically, the ZP of uncoated  
 581 nanoMOFs was positive ( $+23 \pm 3$  mV) at pH 5, whereas it shifted to negative values ( $-15 \pm 3$  mV) at  
 582 pH 7. This was attributed to the presence at the nanoMOFs external surface of both uncoordinated  
 583 iron sites and terminal COOH groups from the nanoMOF linker (trimesic acid, pKa's = 3.16, 3.98, and  
 584 4.85). The ZP values varied after coating with DEX-ALN-PEG copolymers (Figure 3A). At acidic pH  
 585 (<4), the ZP was close to zero ( $-3$  to  $3$  mV) indicating that the surface groups on the nanoMOFs were  
 586 shielded by the coating material. At basic pH (>7) the ZP values of  $-15 \pm 5$  mV were similar to the ones  
 587 previously reported for DEX coatings [37]. Of note, there was no significant variation for ZP values  
 588 obtained with the different DEX-ALN-PEG copolymers, except in the case of the copolymer with the

589 highest PEG content (8) whose ZP values were the closest to zero. This is in line with the protective  
 590 effect of PEG shells on NPs, as previously reported [38]. However, when the amount of DEX-ALN-  
 591 PEG copolymers in the nanoMOFs was reduced, the ZP values at pH >7 tended to approach those of  
 592 uncoated nanoMOFs (Figure 3A).



593

594 **Figure 3.** Effect of surface modification of nanoMOFs by DEX-ALN-PEG copolymers on their  
 595 ZP (A) and amounts of HSA adsorbed (B). Green: uncoated nanoMOF; purple: nanoMOF coated with  
 596 DEX-ALN<sub>75</sub>-PEG<sub>25</sub> 6 (mass ratio DEX-ALN-PEG: nanoMOFs 1:1); orange: nanoMOF coated with  
 597 DEX-ALN<sub>50</sub>-PEG<sub>50</sub> 7 (mass ratio DEX-ALN-PEG: nanoMOFs 1:1); gray: nanoMOF coated with DEX-  
 598 ALN<sub>25</sub>-PEG<sub>75</sub> 8 (mass ratio DEX-ALN-PEG: nanoMOFs 1:1); red: nanoMOF coated with DEX-ALN<sub>50</sub>-  
 599 PEG<sub>50</sub> 7 (mass ratio DEX-ALN-PEG: nanoMOFs 1:2).

600

601 It is well known that surface functionalization strongly influences the biodistribution of the  
 602 nanocarriers [10]. Indeed, after intravenous administration of NPs, plasma proteins readily adsorb  
 603 on the external surface of the NPs, creating the so-called “protein corona”, which considerably affects  
 604 the NPs’ physicochemical properties and *in vivo* fate [39]. To gain further understanding on protein  
 605 adsorption, the interaction of nanoMOFs coated or not with DEX-ALN-PEG with HSA, the most  
 606 abundant protein in human blood plasma, was studied here. Indeed, for many other types of NPs,  
 607 HSA was used as model protein to investigate the capacity of PEG coatings to reduce protein  
 608 adsorption [39]. NanoMOFs coated or not with DEX-ALN-PEG copolymers were incubated with  
 609 HSA aqueous solutions and the adsorbed HSA amounts, expressed as µg/mg of nanoMOFs, were  
 610 determined (Figure 3B). The experiments were carried out with fixed concentrations of nanoMOFs  
 611 (300 µg/mL) and HSA (100 µg/mL) aqueous solutions. Non-adsorbed HSA was recovered in the  
 612 supernatant after centrifugation, followed by quantification using a BCA assay. In the case of  
 613 uncoated nanoMOFs, the amount of adsorbed HSA reached a plateau within 6 h, with around 50 µg  
 614 HSA/mg nanoMOFs (Figure 3B). Surface modification with DEX-ALN-PEG significantly reduced  
 615 HSA adsorption, with ~35 µg HSA/mg nanoMOFs for the case of DEX-ALN<sub>50</sub>-PEG<sub>50</sub> 7 (mass ratio  
 616 DEX-ALN-PEG:nanoMOFs 1:2) coatings. This amount was further reduced to less than 20 µg  
 617 HSA/mg nanoMOFs for the coatings with DEX-ALN<sub>75</sub>-PEG<sub>25</sub> 6, DEX-ALN<sub>50</sub>-PEG<sub>50</sub> 7, and DEX-ALN<sub>25</sub>-  
 618 PEG<sub>75</sub> 8 (mass ratio DEX-ALN-PEG:nanoMOFs 1:1). There results clearly show that the DEX-ALN-  
 619 PEG coatings are able to reduce the adsorption of the model protein HSA.

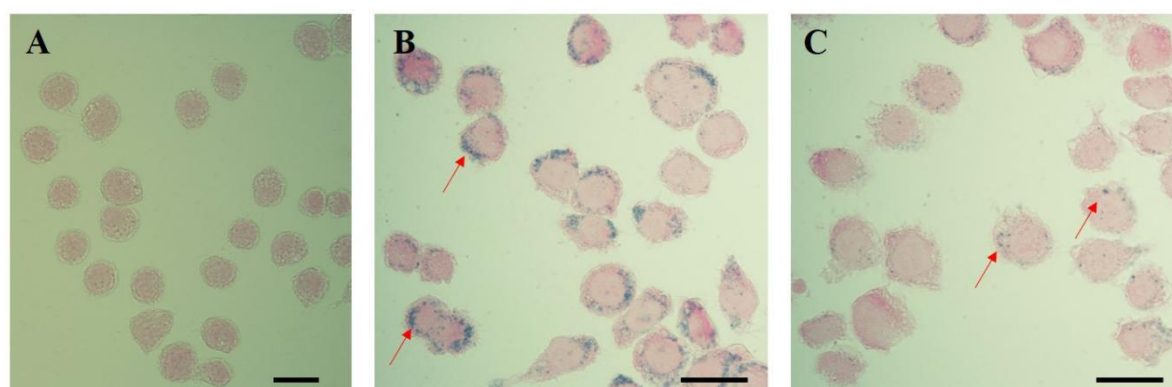
### 620 3.2.3 Macrophage uptake of DEX-ALN-PEG surface modified nanoMOFs

621 The capacity of DEX-ALN-PEG coated nanoMOFs to escape macrophage uptake was evaluated  
 622 on the murine macrophage cell line J774. NanoMOFs were colored using an iron staining procedure  
 623 (see material and methods), allowing their identification inside cells by optical microscopy. To  
 624 complete these qualitative studies, quantitative data on the amounts of nanoMOFs internalized in  
 625 cells were obtained by ICP-MS, after extensive washing to remove the non-associated particles.

626 According to an lactic acid dehydrogenase (LDH) test previously used to study nanoMOF  
627 toxicity [17], it was shown that the particles used here coated or not with DEX-ALN-PEG shells were  
628 nontoxic for the J774 cells up to 100 mg/mL, with more than 80% cell viability. This is in agreement  
629 with previously reported data showing the lack of toxicity of MIL-100(Fe) nanoMOFs [4,5,14,17,40].  
630 Internalization kinetics of nanoMOFs in J774 macrophages were studied and a typical example is  
631 presented in Figure S14 (supplementary material). The amount of internalized uncoated nanoMOFs  
632 was quantified by ICP-MS, showing that after 2 h incubation ~14  $\mu\text{g}$  of uncoated nanoMOFs were  
633 taken up in  $3 \times 10^5$  J774 macrophages, corresponding to around  $1 \times 10^7$  uncoated nanoMOFs/cell and to  
634 47% of the initial uncoated nanoMOFs (Figure S14). Moreover, this amount almost doubled after 4 h  
635 incubation, reaching 23  $\mu\text{g}$  uncoated nanoMOFs/ $3 \times 10^5$  cells (77% of the nanoMOFs), thus  
636 demonstrating that macrophages avidly take up uncoated nanoMOFs. Remarkably, the presence of  
637 the DEX-ALN-PEG coating significantly reduced the nanoMOFs internalization, whatever the  
638 incubation time. For example, there was only less than 3  $\mu\text{g}$  of coated nanoMOFs in  $3 \times 10^5$  J774  
639 macrophages (corresponding to 10% of the initial coated nanoMOFs) after 2 h incubation. Even after  
640 4h incubation, the internalized amount of coated nanoMOFs was still less than 25%.

641 These direct quantification data obtained by ICP MS were supported by optical investigations  
642 of the cells after incubation with the nanoMOFs (Figure 4). Before contact with nanoMOFs, J774  
643 presented a homogeneous morphology with round shapes (Figure 4A). A typical image showing the  
644 massive uptake of uncoated nanoMOFs is presented in Figure 4B. After 2h incubation, the nanoMOFs  
645 appeared clustered inside the macrophages, mostly at their periphery. In contrast, after the same  
646 incubation time, the uptake of DEX-ALN<sub>75</sub>-PEG<sub>25</sub> 6 coated nanoMOFs was dramatically reduced  
647 (Figure 4C).

648

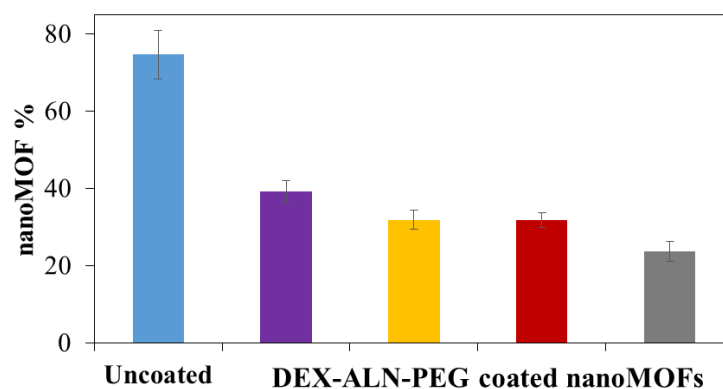


649

650 **Figure 4.** Optical microscopy images showing the effect of DEX-ALN-PEG coatings on J774  
651 macrophage uptake. **A:** Control J774 macrophages with no treatment; **B:** J774 macrophages after 2 h  
652 incubation with 50  $\mu\text{g}/\text{mL}$  uncoated nanoMOFs; **C:** J774 macrophages after 2 h incubation with 50  
653  $\mu\text{g}/\text{mL}$  DEX-ALN<sub>75</sub>-PEG<sub>25</sub> 6 coated nanoMOFs (mass ratio DEX-ALN-PEG:nanoMOFs 1:1). Red  
654 arrows point out nanoMOFs stained using Prussian blue. Scale bar represents 20  $\mu\text{m}$ .

655 The higher uptake of DEX-ALN<sub>75</sub>-PEG<sub>25</sub> 6 coated nanoMOFs after 4 h as compared to 2 h (Figure  
656 S14) could be possibly due to a progressive saturation of the cells and/or a detachment of the coating  
657 in the complex biological media containing proteins or by contact with cell membranes. To further  
658 compare the different DEX-ALN-PEG coatings, an incubation time of 4 h was chosen as it  
659 corresponds to the blood circulation time of PEG-coated nanoparticles [9]. Figure 5 shows the effect  
660 of the DEX-ALN-PEG coatings upon macrophage uptake. The nanoMOFs amounts associated to the  
661 cells were 39, 32 and 24% for DEX-ALN<sub>75</sub>-PEG<sub>25</sub> 6, DEX-ALN<sub>50</sub>-PEG<sub>50</sub> 7, and DEX-ALN<sub>25</sub>-PEG<sub>75</sub> 8,  
662 respectively. This shows that the higher the PEG contents in the coating material, the lower the  
663 nanoMOF uptake.





664

665 **Figure 5.** *In vitro* interaction of nanoMOFs, coated or not with with a J774 macrophage cell line.  
 666 Purple: nanoMOFs coated with DEX-ALN<sub>75</sub>-PEG<sub>25</sub> **6** (mass ratio DEX-ALN-PEG:nanoMOFs 1:1);  
 667 Orange: nanoMOFs coated with DEX-ALN<sub>50</sub>-PEG<sub>50</sub> **7** (mass ratio DEX-ALN-PEG:nanoMOFs 1:1); red:  
 668 nanoMOFs coated with DEX-ALN<sub>50</sub>-PEG<sub>50</sub> **7** (mass ratio DEX-ALN-PEG:nanoMOFs 1:2); gray:  
 669 nanoMOFs coated with DEX-ALN<sub>25</sub>-PEG<sub>75</sub> **8** (mass ratio DEX-ALN-PEG:nanoMOFs 1:1). 50 µg/mL  
 670 nanoMOFs were incubated with 3×10<sup>5</sup> J774 cells for 4 h, then washed to remove the loosely adhering  
 671 particles. After cell lysis, the amount of internalized nanoMOFs was determined by ICP-MS and was  
 672 expressed as a % of the initial amount put in contact with the cells.

673 To the best of our knowledge, these are the first quantitative data on PEG-coated nanoMOF  
 674 uptake by macrophages based on a direct quantification and visualization of the Fe content in the  
 675 cells. In comparison, another recent study dealt with nanoMOF interaction with Raw 246.7  
 676 macrophages [14]. In that case, the MIL-100(Fe) nanoMOFs were coated with PEG by GraftFast,  
 677 whereas a radiolabeled drug, tritiated gemcitabine monophosphate, was incorporated into the  
 678 particles. In the presence of coated particles, the detected amount of drug in the cells was reduced, as  
 679 opposed to uncoated ones. However, this study did not take into account drug release during  
 680 incubation with the cells, which may have influenced the quantity of drug detected as permeated into  
 681 the cells [19].

## 682 5. Conclusions

683 DEX-ALN-PEG copolymers were successfully synthesized, controlling both the PEG and ALN  
 684 grafting densities ranging from 75:25 to 25:75 ratios. They spontaneously adhered onto the external  
 685 surface of nanoMOFs in aqueous media, forming a stable coating. In turn, the coating ensured the  
 686 stability of the nanoMOFs upon storage and enabled to reduce by a 3 fold the *in vitro* uptake by  
 687 macrophages. Further studies will deal with the further engineering of the coating by grafting specific  
 688 ligands and/or fluorescent molecules. The *in vivo* fate of DEX-ALN-PEG functionalized nanoMOFs  
 689 will be investigated.

690 **Supplementary Materials:** The following are available online at [www.mdpi.com/xxx/s1](http://www.mdpi.com/xxx/s1), Figure S1: <sup>1</sup>H NMR  
 691 spectrum (600 MHz, D<sub>2</sub>O, 25 °C) for compound **3**, Figure S2: <sup>1</sup>H NMR spectrum (300 MHz, D<sub>2</sub>O, 25 °C) for  
 692 compound **4**, Figure S3: <sup>1</sup>H NMR spectrum (600 MHz, D<sub>2</sub>O, 25 °C) for DEX-PC **5**, Figure S4: <sup>1</sup>H NMR spectrum  
 693 (600 MHz, D<sub>2</sub>O, 25 °C) for DEX-ALN<sub>75</sub>-PEG<sub>25</sub> **6**, Figure S5: <sup>1</sup>H NMR spectrum (600 MHz, D<sub>2</sub>O, 25 °C) for DEX-  
 694 ALN<sub>50</sub>-PEG<sub>50</sub> **7**, Figure S6: <sup>1</sup>H NMR spectrum (600 MHz, D<sub>2</sub>O, 25 °C) for DEX-ALN<sub>25</sub>-PEG<sub>75</sub> **8**, Figure S7: <sup>13</sup>C NMR  
 695 spectrum (150 MHz, D<sub>2</sub>O, 25 °C) for compound **3**, Figure S8: <sup>13</sup>C NMR spectrum (75 MHz, D<sub>2</sub>O, 25 °C) for  
 696 compound **4**, Figure S9: <sup>13</sup>C NMR spectrum (150 MHz, D<sub>2</sub>O, 25 °C) for DEX-PC **5**, Figure S10: <sup>31</sup>P NMR spectrum  
 697 (242.9 MHz, D<sub>2</sub>O, 25 °C) for compound **3**, Figure S11: <sup>31</sup>P NMR spectrum (242.9 MHz, D<sub>2</sub>O, 25 °C) for DEX-ALN<sub>75</sub>-  
 698 PEG<sub>25</sub> **6**, Figure S12: <sup>31</sup>P NMR spectrum (242.9 MHz, D<sub>2</sub>O, 25 °C) for DEX-ALN<sub>50</sub>-PEG<sub>50</sub> **7**, Figure S13: <sup>31</sup>P NMR  
 699 spectrum (242.9 MHz, D<sub>2</sub>O, 25 °C) for DEX-ALN<sub>25</sub>-PEG<sub>75</sub> **8**, Figure S14: Interaction of nanoMOFs, coated or not  
 700 with DEX-ALN<sub>25</sub>-PEG<sub>75</sub> **8**, with J774 macrophages. 50 µg/mL nanoMOFs were incubated with 3×10<sup>5</sup> J774 cells for  
 701 2 h and 4 h, respectively.

**702 Author Contributions:**

703 The author(s) have made the following declarations about their contributions:

704 Conceived and designed the experiments: RG, AVB, DD

705 Performed the experiments: GC, JQ, AA, XL, MMM, DF, JMCS, BMA, JRE

706 Contributed reagents/materials/analysis tools: GC, AA, CL, XL, JQ, MMM, JMCS, DD, RG, AVB

707 Performed data analysis: GC, RG, AVB, DD, CL, XL, MMM, JMCS

708 Wrote the paper: RG, AVB, XL, GC

709 **Funding:** Financial support for this work was provided by the European Union through FP7-PEOPLE-2013-ITN  
710 (<http://itn-cyclonhit.eu>) project (Grant Agreement no. 608407), the French Agence Nationale de la Recherche  
711 (ANR-14-CE08-0017 and ANR-16-CE18-0018), the Spanish Ministry of Economy and Competitiveness (Grant  
712 CTQ2017-90050-R) and by government of Principado de Asturias through the project FC-GRUPIN-712  
713 IDI/2018/000166. This work was also supported by a public grant overseen by the French National Research  
714 Agency (ANR) as part of the “Investissements d’Avenir” program (Labex NanoSaclay, ANR-10-LABX-0035).

715 **Acknowledgments:** We acknowledge Dr. Doru Constantin for help with XRPD experiments. We are grateful to  
716 Ludivine Houel Renault for help with the cell culture facility in Centre Laser de l’Université Paris-Sud (CLUPS).  
717 This work has benefited from the facilities and expertise of the Liquid Chromatography Platform (Institut de  
718 Chimie de Lyon) for the characterization of polymers.

719 **Conflicts of Interest:** The authors declare no conflict of interest.

**720 References**

- 721 1. Hoskins, B.F.; Robson, R. Infinite polymeric frameworks consisting of three dimensionally linked rod-  
722 like segments. *J. Am. Chem. Soc.* **1989**, *111*, 5962–5964.
- 723 2. Horcajada, P.; Gref, R.; Baati, T.; Allan, P.K.; Maurin, G.; Couvreur, P.; Ferey, G.; Morris, R. E.; Serre, C.  
724 Metal-organic frameworks in biomedicine. *Chem. Rev.* **2012**, *112*, 1232–1268.
- 725 3. Yuan, S.; Feng, L.; Wang, K.; Pang, J.; Bosch, M.; Lollar, C.; Sun, Y.; Qin, J.; Yang, X.; Zhang, P. Stable  
726 metal-organic frameworks: design, synthesis, and applications. *Adv. Mater.* **2018**, *30*, 1–35.
- 727 4. Horcajada, P.; Chalati, T.; Serre, C.; Gillet, B.; Sebrie, C.; Baati, T.; Eubank, E.F.; Heurtaux, D.; Clayette,  
728 P.; Kreuz, C.; Chang J. S.; Hwang Y. K.; Marsaud V.; Bories P. N.; Cynober L.; Gil S.; Ferey G.; Couvreur  
729 P.; Gref R., Porous metal–organic-framework nanoscale carriers as a potential platform for drug  
730 delivery and imaging. *Nat. Mater.* **2010**, *9*, 172–178.
- 731 5. Baati, T.; Njim, L.; Neffati, F.; Kerkeni, A.; Bouttemi, M.; Gref, R.; Najjar, M.F.; Zakhama, A.; Couvreur,  
732 P.; Serre C. In depth analysis of the *in vivo* toxicity of nanoparticles of porous iron(III) metal-organic  
733 frameworks. *Chem. Sci.* **2013**, *4*, 1597–1607.
- 734 6. Agostoni, V.; Chalati, T.; Horcajada, P.; Willaime, H.; Anand, R.; Semiramoth, N.; Baati, T.; Hall, S.;  
735 Maurin, G.; Chacun, H. An improved anti-HIV activity of NRTI via metal-organic frameworks  
736 nanoparticles. *Adv. Healthc. Mater.* **2013**, *2*, 1630–1637.
- 737 7. Simon-Yarza, T.; Giménez-Marqués, M.; Mrimi, R.; Mielcarek, A.; Gref, R.; Horcajada, P.; Serre, C.;  
738 Couvreur, P. A smart metal-organic framework nanomaterial for lung targeting. *Angew. Chem. Int. Ed.*  
739 **2017**, *56*, 15565–15569.

- 740 8. Simon-Yarza, M.T.; Baati, T.; Paci, A.; Lesueur, L.L.; Seck, A.; Chiper, M.; Gref, R.; Serre, C.; Couvreur,  
741 P.; Horcajada, P. Antineoplastic Busulfan encapsulated in metal organic framework nanocarrier: first *in*  
742 *vivo* results. *J. Mater. Chem. B* **2016**, *4*, 585–588.
- 743 9. Gref, R.; Minamitake, Y.; Peracchia, M.T.; Trubetskoy, V.; Torchilin, V.; Langer, R. Biodegradable long-  
744 circulating polymeric nanospheres. *Science* **1994**, *263*, 1600–1603.
- 745 10. Gref, R.; Domb, A.; Quellec, P.; Blunk, T.; Müller, R.H.; Verbavatz, J.M.; Langer, R. The controlled  
746 intravenous delivery of drugs using PEG-coated sterically stabilized nanospheres. *Adv. Drug Deliv. Rev.*  
747 **1995**, *16*, 215–233.
- 748 11. Barenholz, Y. Doxil® - The first FDA-approved nano-drug: lessons learned. *J. Control. Release* **2012**, *160*,  
749 117–134.
- 750 12. Agostoni, V.; Horcajada, P.; Noiray, M.; Malanga, M.; Aykaç, A.; Jicsinszky, L.; Vargas-Berenguel, A.;  
751 Semiramoth, N.; Daoud-Mahammed, S.; Nicolas, V.; et al. A “green” strategy to construct non-covalent,  
752 stable and bioactive coatings on porous MOF nanoparticles. *Sci. Rep.* **2015**, *5*, 7925.
- 753 13. Zhang, H.H.; Hu, H.; Zhang, H.H.; Dai, W.; Wang, X.; Wang, X.; Zhang, Q. Effects of PEGylated  
754 paclitaxel nanocrystals on breast cancer and its lung metastasis. *Nanoscale* **2015**, *7*, 10790–10800.
- 755 14. Giménez-Marqués, M.; Bellido, E.; Berthelot, T.; Simón-Yarza, T.; Hidalgo, T.; Simón-Vázquez, R.;  
756 González-Fernández, Á.; Avila, J.; Asensio, M.C.; Gref, R.; et al. GraftFast surface engineering to improve  
757 MOF nanoparticles furtiveness. *Small* **2018**, *14*, 1801900.
- 758 15. Chen, D.; Yang, D.; Dougherty, C.A.; Lu, W.; Wu, H.; He, X.; Cai, T.; Van Dort, M.E.; Ross, B.D.; Hong,  
759 H. *In vivo* targeting and positron emission tomography imaging of tumor with intrinsically radioactive  
760 metal-organic frameworks nanomaterials. *ACS Nano* **2017**, *11*, 4315–4327.
- 761 16. Zimpel, A.; Preiß, T.; Röder, R.; Engelke, H.; Ingrisch, M.; Peller, M.; Rädler J.O.; Wagner, E.; Bein T.;  
762 Lächelt, U.; et al. Imparting functionality to MOF nanoparticles by external surface selective covalent  
763 attachment of polymers. *Chem. Mater.* **2016**, *28*, 3318–3326.
- 764 17. Li, X.; Semiramoth, N.; Hall, S.; Tafani, V.; Josse, J.; Laurent, F.; Salzano, G.; Foulkes, D.; Brodin, P.;  
765 Majlessi, L.; et al. Compartmentalized encapsulation of two antibiotics in porous nanoparticles: an  
766 efficient strategy to treat intracellular infections. *Part. Part. Syst. Charact.* **2019**, *36*, 1800360.
- 767 18. Di Nunzio, M.R.; Agostoni, V.; Cohen, B.; Gref, R.; Douhal, A. A “ship in a bottle” strategy to load a  
768 hydrophilic anticancer drug in porous metal organic framework nanoparticles: Efficient encapsulation,  
769 matrix stabilization, and photodelivery. *J. Med. Chem.* **2014**, *57*, 411–420.
- 770 19. Rodriguez-Ruiz, V.; Maksimenko, A.; Anand, R.; Monti, S.; Agostoni, V.; Couvreur, P.; Lampropoulou,  
771 M.; Yannakopoulou, K.; Gref, R. Efficient “green” encapsulation of a highly hydrophilic anticancer drug  
772 in metal-organic framework nanoparticles. *J. Drug Target.* **2015**, *23*, 759–767.
- 773 20. Agostoni, V.; Anand, R.; Monti, S.; Hall, S.; Maurin, G.; Horcajada, P.; Serre, C.; Bouchemal, K.; Gref, R.

- 774 Impact of phosphorylation on the encapsulation of nucleoside analogues within porous iron(III) metal-  
775 organic framework MIL-100(Fe) nanoparticles. *J. Mater. Chem. B* **2013**, *1*, 4231–4242.
- 776 21. Simon-Yarza, T.; Baati, T.; Neffati, F.; Njim, L.; Couvreur, P.; Serre, C.; Gref, R.; Najjar, M.F.; Zakhama,  
777 A.; Horcajada, P. *In vivo* behavior of MIL-100 nanoparticles at early times after intravenous  
778 administration. *Int. J. Pharm.* **2016**, *511*, 1042–1047.
- 779 22. Perrin, D.D.; Armarego, W.F.L. *Purification of Laboratory Chemicals*, 3rd ed., Pergamon: Oxford, 1989..
- 780 23. Alemán, E.A.; Pedini, H.S.; Rueda, D. Covalent bond-based immobilization approaches for single-  
781 molecule fluorescence. *Chembiochem* **2009**, *10*, 2862–2866.
- 782 24. Kuil, J.; Branderhorst, H.M.; Pieters, R.J.; De Mol, N.J.; Liskamp, R.M.J. ITAM-derived phosphopeptide-  
783 containing dendrimers as multivalent ligands for Syk tandem SH2 domain. *Org. Biomol. Chem.* **2009**, *7*,  
784 4088–4094.
- 785 25. Grandjean, C.; Boutonnier, A.; Guerreiro, C.; Fournier, J.M.; Mulard, L.A. On the preparation of  
786 carbohydrate-protein conjugates using the traceless Staudinger ligation. *J. Org. Chem.* **2005**, *70*, 7123–  
787 7132.
- 788 26. Ke, J.; Dou, H.; Zhang, X.; Uhagaze, D.S.; Ding, X.; Dong, Y. Determination of pKa values of alendronate  
789 sodium in aqueous solution by piecewise linear regression based on acid-base potentiometric titration.  
790 *J. Pharm. Anal.* **2016**, *6*, 404–409.
- 791 27. Semple, J.E.; Sullivan, B.; Vojkovsky, T.; Sill, K.N. Synthesis and facile end-group quantification of  
792 functionalized PEG azides. *J. Polym. Sci. Part A Polym. Chem.* **2016**, *54*, 2888–2895.
- 793 28. Sun, G.; Lin, X.; Wang, Z.; Feng, Y.; Xu, D.; Shen, L. PEGylated inulin as long-circulating pharmaceutical  
794 carrier. *J. Biomater. Sci. Polym. Ed.* **2011**, *22*, 429–441.
- 795 29. Ostović, D.; Stelmach, C.; Hulshizer, B. Formation of a chromophoric complex between alendronate and  
796 copper(II) ions. *Pharm. Res.* **1993**, *10*, 470–472.
- 797 30. Oms, O.; Yang, S.; Salomon, W.; Marrot, J.; Dolbecq, A.; Rivière, E.; Bonnefont, A.; Ruhlmann, L.;  
798 Mialane, P. Heteroanionic materials based on copper clusters, bisphosphonates, and polyoxometalates:  
799 magnetic properties and comparative electrocatalytic NO<sub>x</sub> reduction studies. *Inorg. Chem.* **2016**, *55*, 1551–  
800 1561.
- 801 31. Biaglow, J.E.; Manevich, Y.; Uckun, F.; Held, K.D. Quantitation of hydroxyl radicals produced by  
802 radiation and copper-linked oxidation of ascorbate by 2-deoxy-D-ribose method. *Free Radic. Biol. Med.*  
803 **1997**, *22*, 1129–1138.
- 804 32. Barceloux, D.G. Copper. *Clin. Toxicol.* **1999**, *37*, 217–230.
- 805 33. Notni, J.; Wester, H.J. A practical guide on the synthesis of metal chelates for molecular imaging and  
806 therapy by means of click chemistry. *Chem. - A Eur. J.* **2016**, *22*, 11500–11508.

- 807 34. Su, Y.; Li, L.; Wang, H.; Wang, X.; Zhang, Z. All-in-One azides: empowered click reaction for *in vivo*  
808 labeling and imaging of biomolecules. *Chem. Commun.* **2016**, *52*, 2185–2188.
- 809 35. Aykaç, A.; Noiray, M.; Malanga, M.; Agostoni, V.; Casas-Solvas, J.M.; Fenyvesi, É.; Gref, R.; Vargas-  
810 Berenguel, A. A non-covalent “click chemistry” strategy to efficiently coat highly porous MOF  
811 nanoparticles with a stable polymeric shell. *Biochim. Biophys. Acta - Gen. Subj.* **2017**, *1861*, 1606–1616.
- 812 36. Zhu, X.; Gu, J.; Wang, Y.; Li, B.; Li, Y.; Zhao, W.; Shi, J. Inherent anchorages in UiO-66 nanoparticles for  
813 efficient capture of alendronate and its mediated release. *Chem. Commun.* **2014**, *50*, 8779–8782.
- 814 37. Lemarchand, C.; Gref, R.; Lesieur, S.; Hommel, H.; Vacher, B.; Besheer, A.; Maeder, K.; Couvreur, P.  
815 Physico-chemical characterization of polysaccharide-coated nanoparticles. *J. Control. Release* **2005**, *108*,  
816 97–111.
- 817 38. Rouzes, C.; Gref, R.; Leonard, M.; De Sousa Delgado, A.; Dellacherie, E. Surface modification of  
818 poly(lactic acid) nanospheres using hydrophobically modified dextrans as stabilizers in an o/w  
819 emulsion/evaporation technique. *J. Biomed. Mater. Res.* **2000**, *50*, 557–565.
- 820 39. Gref, R.; Lück, M.; Quellec, P.; Marchand, M.; Dellacherie, E.; Harnisch, S.; Blunk, T.; Müller, R.H.  
821 “Stealth” corona-core nanoparticles surface modified by polyethylene glycol (PEG): Influences of the  
822 corona (PEG chain length and surface density) and of the core composition on phagocytic uptake and  
823 plasma protein adsorption. *Colloids Surf. B Biointerfaces* **2000**, *18*, 301–313.
- 824 40. Bellido, E.; Hidalgo, T.; Lozano, M.V.; Guillevic, M.; Simón-Vázquez, R.; Santander-Ortega, M.J.;  
825 González-Fernández, Á.; Serre, C.; Alonso, M.J.; Horcajada, P. Heparin-engineered mesoporous iron  
826 metal-organic framework nanoparticles: toward stealth drug nanocarriers. *Adv. Healthc. Mater.* **2015**, *4*,  
827 1246–1257.

828